EFFECTS OF BLADE CONFIGURATION ON FLOW DISTRIBUTION AND POWER OUTPUT OF A ZEPHYR VERTICAL AXIS WIND TURBINE

BY

JOHN OVIEMUNO AJEDEGBA

A THESIS SUBMITTED IN PARTIAL FULFILLMENT
OF THE REQUIREMENTS FOR THE DEGREE OF

MASTER OF APPLIED SCIENCE

IN

MECHANICAL ENGINEERING

THE FACULTY OF ENGINEERING AND APPLIED SCIENCE

UNIVERSITY OF ONTARIO INSTITUTE OF TECHNOLOGY

JULY, 2008

CERTIFICATE OF APPROVAL

Submitted by: John Oviemuno Ajedegba Student #: 100333647

In partial fulfillment of the requirements for the degree of

Master of Applied Science in Mechanical Engineering

Date of Defense (if applicable)

Effects of Blade Configuration on Flow Distribution and Power Output of a Zephyr Vertical Axis Wind Turbine

The undersigned certify that they recommend this thesis to the Office of Graduate Studies for acceptance:

Chair of Examining Committee	Signature	2008/08/19
External Examiner	Signature	(2008/08/19)
Member of Examining Committee	Signature	(2008/08/19)
Member of Examining Committee	Signature	(2008/08/19)

As research supervisor for the above student, I certify that I have read the following defended thesis, have approved changes required by the final examiners, and recommend it to the Office of Graduate Studies for acceptance:

Name of Research Supervisor	Signature of Research Supervisor	(2008/08/19)
Name of Research Supervisor	Signature of Research Supervisor	(2008/08/19)

ABSTRACT

Worldwide interest in renewable energy systems has increased dramatically, due to environmental concerns like climate change and other factors. Wind power is a major source of sustainable energy, and can be harvested using both horizontal and vertical axis wind turbines. This thesis presents studies of a vertical axis wind turbine performance for applications in urban areas. Numerical simulations with FLUENT software are presented to predict the fluid flow through a novel Zephyr vertical axis wind turbine (VAWT). Simulations of air flow through the turbine rotor were performed to analyze the performance characteristics of the device. Major blade geometries were examined. A multiple reference frame (MRF) model capability of FLUENT was used to express the dimensionless form of power output of the wind turbine as a function of the wind freestream velocity and the rotor's rotational speed. A sliding mesh model was used to examine the transient effects arising from flow interaction between the stationary components and the rotating blades. The simulation results exhibit close agreement with a stream-tube momentum model.

ACKNOWLEDGMENT

From the deepest part of his heart, I feel indebted to my co-supervisors, Professor G. F. Naterer, and Professor M. Rosen, founding dean of FEAS, UOIT for their invaluable encouragement and guidance throughout this thesis and study period. This author sincerely and specifically thanks his co-supervisors for their continuous patience and trust for not given up on me.

The author would also like to express his gratitude to Mr. Ed Tsang, the managing director of Zephyr Alternative Power Inc., Toronto, for his industrial encouragement and support, as well as the Natural Science and Engineering Research Council of Canada for financial support.

I am also grateful to Dr. E. O. B. Ogedengbe of CANMET Energy Technology Centre - Ottawa for his prayers and worthy counsellorship.

TABLE OF CONTENTS

LIST OF FIGURES

FIGURES

LIST OF TABLES

NOMENCLATURE

L	Lift force [N]
C_L	Lift coefficient [-]
A	Blade surface area [m^2]
D	Drag force [N]
C_d	Drag coefficient [-]
U, U_∞	Wind speed [m/s]
V_r ,	Relative wind speed [m/s]
Ω	Rotor angular speed [rad/s]
r, R	Radius of rotors [m]
ρ	Air density [kg/m^3]
ϕ	Flow angle [radian]
F_T	Tangential force [N]
F_N	Normal force [N]
P	Static pressure [N/m^2]
K_p	Pressure coefficient [-]
Re	Reynolds number [-]
γ	Kinematics viscosity [kg/m/s]
μ	Fluid viscosity [kg/m/s]
δ	Blade solidity [-]
B, N	Number of rotor blades [-]
λ , TSR	Tip speed ratio [-]
P_t	Turbine output power [watts]
V_0	Downstream wind velocity [m/s]
C_p	Power coefficient or rotor efficiency [-]
P_0	Initial pressure [N/m^2]

a	Axial induction factor [-]
α	Angle of attack [radian]
β	Azimuth angle [radian]
Q	Torque [Nm]
Q_L	Lift torque contribution [Nm]
Q_d	Drag torque contribution [Nm]
p_d	Downwind pressure of rotor [N/m^2]
p^u	Upwind pressure of rotor [N/m^2]
p_0	Pressure of undisturbed air [N/m^2]
u_w	Axial wind velocity at far wake [m/s]
$\dot{m}$	Mass flow rate of air [kg/s]
C_N	Normal force coefficient [-]
C_T	Normal thrust coefficient [-]
P_d	Dynamic pressure [N/m^2]
$\vec{T}$	Torque or moment vector [Nm]
$\vec{r_c}$	Vector from the centre of rotor [m]
$\vec{F_p}$	Pressure moment [Nm]
$\vec{F_v}$	Viscous moment [Nm]
d_r	Rotor diameter [m]
h	Rotor height [m]
HAWT	Horizontal axis wind turbine
VAWT	Vertical axis wind turbine

Chapter 1

1.0 INTRODUCTION

World electricity consumption is over 16,000 billion kWh annually; about 70% is generated from the burning of fossil fuels. The remaining percentage is obtained from other sources including hydropower, geothermal, biomass, solar, wind and nuclear energy [1]. Of this 30%, only about 0.3% is produced by converting the kinetic energy of wind into electricity. In view of global interest to reduce greenhouse gas emissions and provide sustainable energy that will meet rising demand for energy services, efforts are underway to supplement our energy base with renewable energy. This increasing demand for renewable energy resources and global concern about pollution and environmental degradation are consequences of our dependence on fossil fuels. Wind energy has been identified as a promising renewable option. It is an ancient technology, which only recently has become a promising large–scale source of power. Beside simple and cheap construction, its environmentally benign characteristics account for its growing importance. Policies are being formulated by many nations today to ensure that wind power has a growing role in future energy supplies.

Wind power is the world's fastest growing renewable energy resource. This pace has been maintained in the last five years consecutively [2, 3]. Among the European nations, by 2010 the growth of this renewable resource is estimated to be at approximately 22 percent of total renewable energy generation [3].

1.1 BACKGROUND ON WIND POWER

Sustainable energy is needed, but the question is how to make the selection among all the alternatives. For instance, when should wind energy be chosen over solar energy or geothermal? Considering the land area occupied by a university like UOIT, an installed circular solar collector with an area of 1 square meter could give an average of about 7.0 KWh/day; while a vertical axis wind turbine (VAWT) covering the same area could yield about 4.5 KWh/day (estimate based on numbers from *Thirty-Year Average of Monthly Solar Radiation*) [35]. However, solar power is generally more expensive per Watt than wind. A study conducted with a renewable energy recourses (RES) cost comparison has shown that the cost of wind and solar over a period of one year yielded $12.24 per Watt for solar, against $7.02 for wind [2]. In this example wind power is a more viable option. Besides cost, other benefits of wind power are its attractiveness as an alternative power source for both large utilities, and small scale and distributed power generation applications. The following list briefly outlines some of its main advantages.

1. Clean and Inexhaustible Resource: Wind power produces little or no emissions of GHGs during its operation. There are emissions associated with the full life cycle, however. For instance, a past study revealed that a single 1 MW wind turbine operating for 365 days accounts for about 1,500 tons of carbon dioxide, 6.5 tons of sulphur dioxides, 3.2 tons

of nitrogen oxides, and 60 pounds of mercury [3], mainly by indirect manufacturing of components to build wind systems.

2. Modular and Scalable Technology: This is one of the most useful benefits of wind energy that favors its development, i.e., its self contained components. It finds applications in both large wind farms and distributed power generation. A VAWT is useful in this sense because its scalable size is convenient for roof–top installation. The load on the power grid and associated costs are therefore reduced or eliminated.

3. Energy Price Stability: Over–reliance on fossil fuels is contributing to energy price instability, due to the market forces of supply and demand. By diversifying the energy mix, wind energy will reduce the dependency on fossil fuels.

4. Wind for Clean Fuel (Hydrogen): In addition to its capacity for generating electricity, wind power could be used together with electrolysis to produce hydrogen (see fig. 1.1). The US Department of Energy has found wind energy to be a promising source for generating hydrogen [3]. Hydrogen is a clean energy carrier, and could thus be used as a future fuel. Atomic Energy of Canada (AECL) and the University of Ontario Institute of Technology (UOIT) are leading a research initiative to use heat from a

nuclear plant for thermochemical splitting of water into hydrogen and oxygen. This hydrogen production means through an electrolysis process illustrates the flexibility of hydrogen delivered from any wind site.

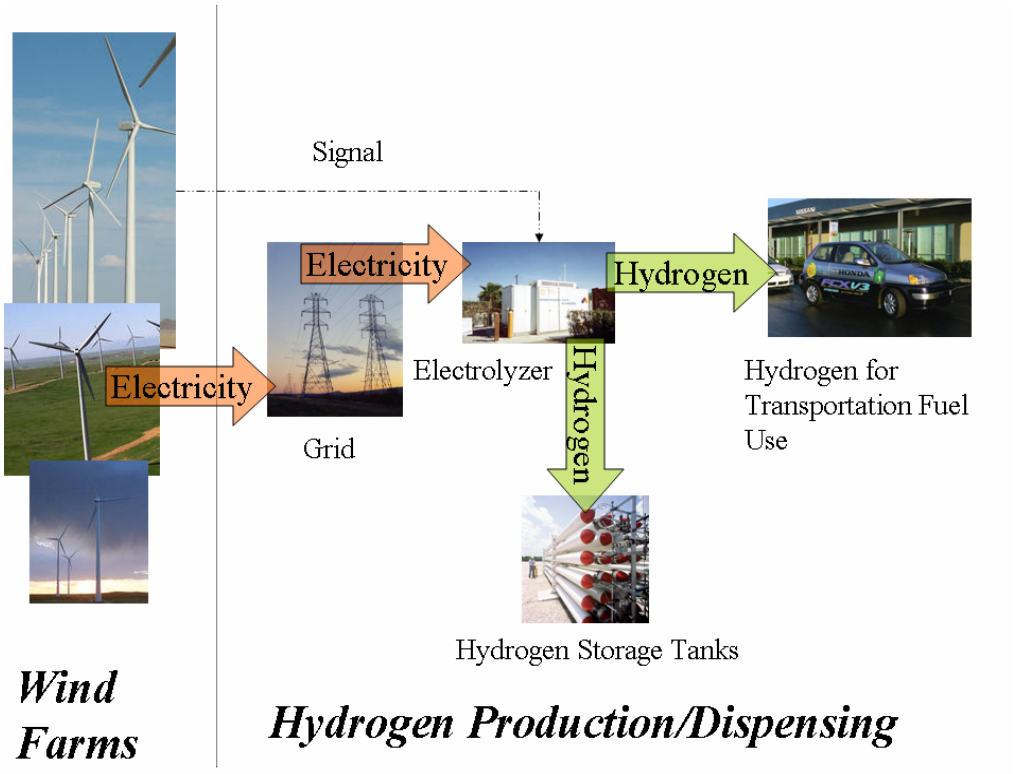

Fig 1.1: Wind power for hydrogen production. www.wind-hydrogen.com

According to the DOE studies, wind hydrogen can be generated for prices ranging from $5.55/kg in the near–term to $2.27/kg in the long–term. [2]. This will place wind energy generation as a leading renewable energy resource in the future.

1.2 Worldwide Growth in Wind Power

There is rapid growth in wind power development globally. This utilization of wind for electricity generation is expanding quickly, due largely to technological improvements, industry maturation and an increasing concern with greenhouse emissions associated with burning of fossil fuels. The Association of Wind Energy Generation [2] has predicted this trend will continue as there is much opportunity to grow this resource internationally. Given the enormous wind resources, only a small portion of the useable wind potential is being utilized presently. Government and electrical industry regulations, as well as government incentives, have a large role in determining how quickly wind power will be adopted.

In Ontario, Canada, for instance, government initiatives such as the Better Buildings Partnership in Toronto encourage and facilitate the development of small turbines in building designs. This particular program offers incentives up to $13,000 to encourage residential developers to “build green”. Across the U.S. in 2006, wind turbine installation capacity has grown from about 9,000 MW to 11,600 MW [3]. European countries have also widely harnessed this energy resource. Germany, Denmark, and Spain are notable users of wind power. Denmark generates 20% of its electricity through wind turbines. The UK has the largest wind energy resources and it is set for large expansion of this clean energy source by taking advantage of the European market economies of scale to bring down the price of wind energy [10]. Installed worldwide capacity of wind power by the end of 2007 was nearly 100,000 MW [4]. Effective policies will help improve the incentives

and ensure that wind power can compete fairly with other fuel sources in the electricity market.

1.2.1 Installed Wind Power Capacity

Report has shown that, one in every three nations is poised to generate a significant portion of its electricity demand from wind energy resources [3]. This is driven by growing concerns regarding climate change and energy security. Over 13 countries are exceeding 1,000 megawatts of installed wind electricity–generating capacity [4]. This is contributing to the growth in both technology and the global wind energy market. The current global installed wind power capacity reached about 100,000 megawatts in March 2008 [4]. In 2002, the total global wind generating capacity was about 31,000 MW, and it provided about 65 billion kWh of electricity annually. In 2004, the capacity of wind energy grew to a level of about 48,000 MW. Of this amount, European nations account for 72% of the total installed capacity, while other countries are taking steps to expand in these large-scale commercial markets. In the world, more than 50 countries now contribute to the global wind market, which has employed many companies. Among these 50 contributing nations to the wind energy market, the primary countries which take up most of the wind energy market are Denmark, Germany, Spain, U.S., Indian, Italy, Netherlands, United Kingdom, France, Portugal and Canada.

Country	Cumulative installed (MW) 2001	Cumulative installed (MW) 2002	Cumulative installed (MW) 2003	Cumulative installed (MW) 2004	Growth rate 2003-2004 %
Germany	8,734	11,968	14,612	16,649	13.90%
Spain	3,550	5,043	6,420	8,263	28.70%
USA	4,245	4,674	6,361	6,750	6.10%
Denmark	2,456	2,880	3,076	3,083	0.20%
India	1,456	1,702	2,125	3,000	41.20%
Italy	700	806	922	1,261	36.70%
Netherlands	523	727	938	1,081	15.30%
Japan	357	486	761	991	30.20%
UK	525	570	759	889	17.10%
P.R. China	406	473	571	769	34.70%
Total	**22,952**	**29,329**	**36,545**	**42,735**	**16.90%**

Table 1.1: Wind power growth rate (cumulative installed in MW) [5]

Table 1.1 shows a review of the years 2001-2004 and the cumulative installed capacity of wind turbines in the global wind energy growth rate. European nations are leaders in the wind energy market and its development. Germany has the largest cumulative capacity, both in Europe and worldwide, with a total of 16,649 MW by the end of the year 2004. Recently, the European Wind Energy

Association has revised its wind capacity projections for 2010 from $4x10^4$ MW to $6x10^4$ MW.

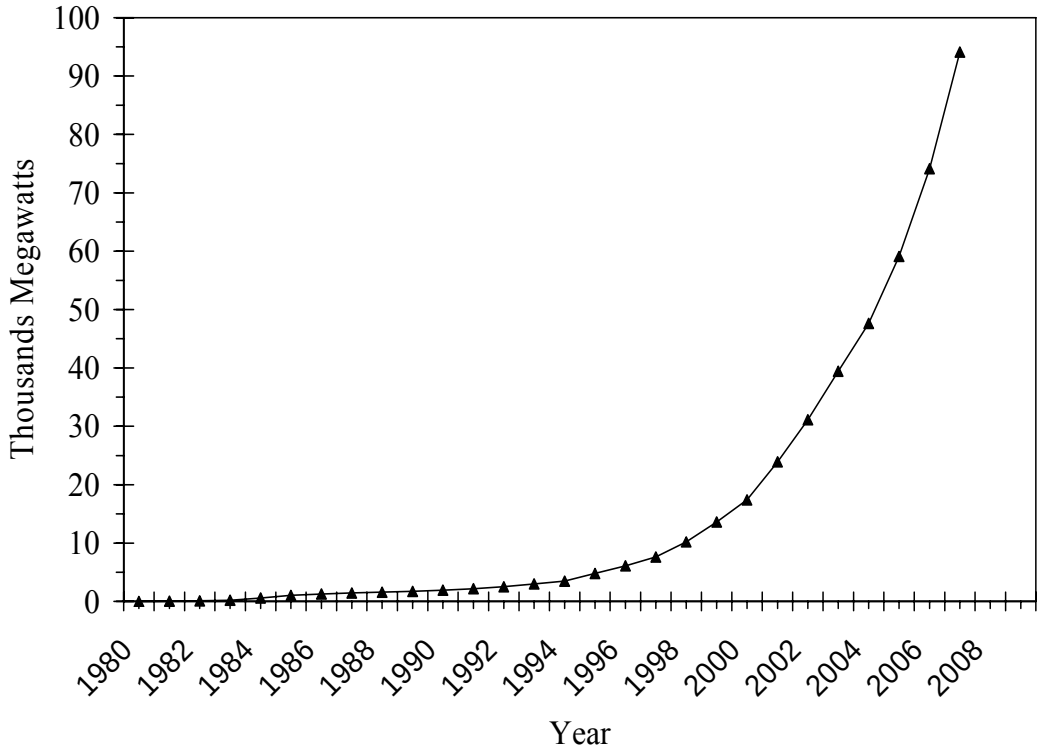

Figure 1.3: Global installed wind energy capacity [4]

There is a rising need for continuous development of wind power. Figure 1.3 illustrates that almost 100,000 MW of wind power is currently installed cumulatively. The Renewable Energy Law (REL), adopted by most developed countries is a boost to encouraging wind energy growth. Most other developing nations of the world have completed a policy formulation that will enable similar measures as the developed countries for full implementation and development of this renewable energy resource. In Africa, Morocco and Egypt are leading in the

number of installations. Figure 1.3 shows the rapid growth of installations. In 2004, the U. S. experienced a slight reduction during the global growth. Today its total cumulative installed capacity has reached about 16,818 MW.

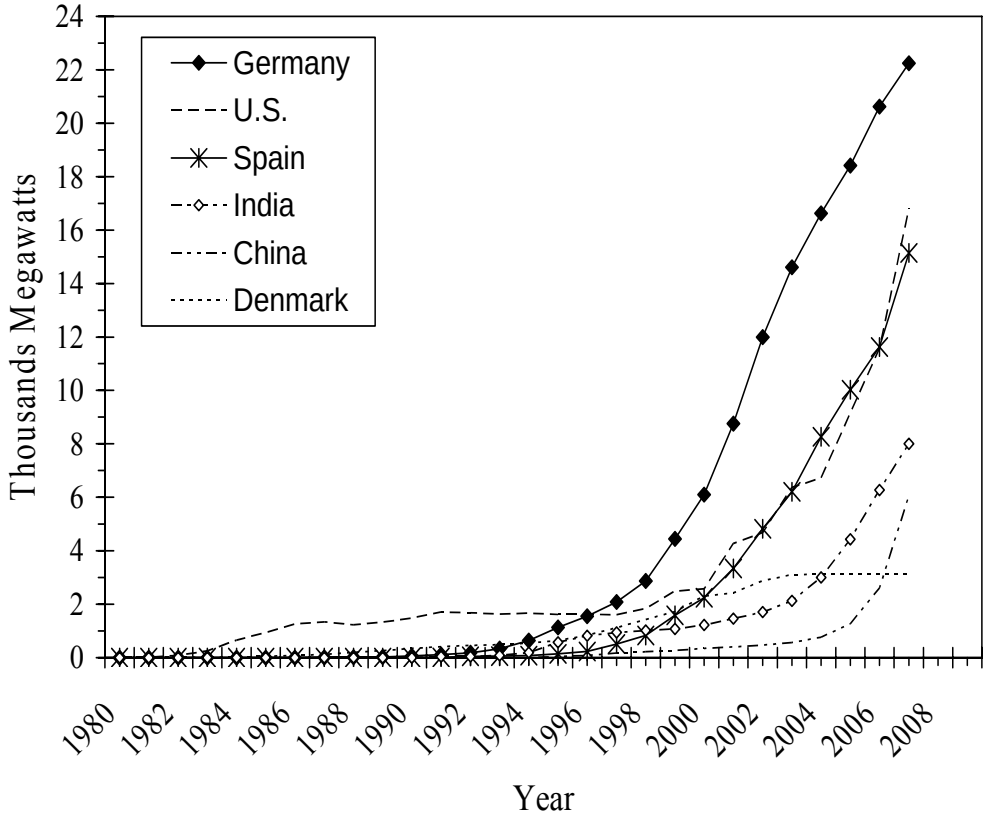

Figure 1.4: Top cumulative installed wind power capacities (World, 1980-2007) [4]

In recent years, the cumulative generating capacity is mainly dominated by six countries: Germany (25%), U.S. (18%), Spain (16%), Denmark (3%), China (6%), and India (8%). Together they account for 76% of the total (see Figs. 1.4 and 1.5). This is sufficient to meet the electricity needs of over 60 million average homes.

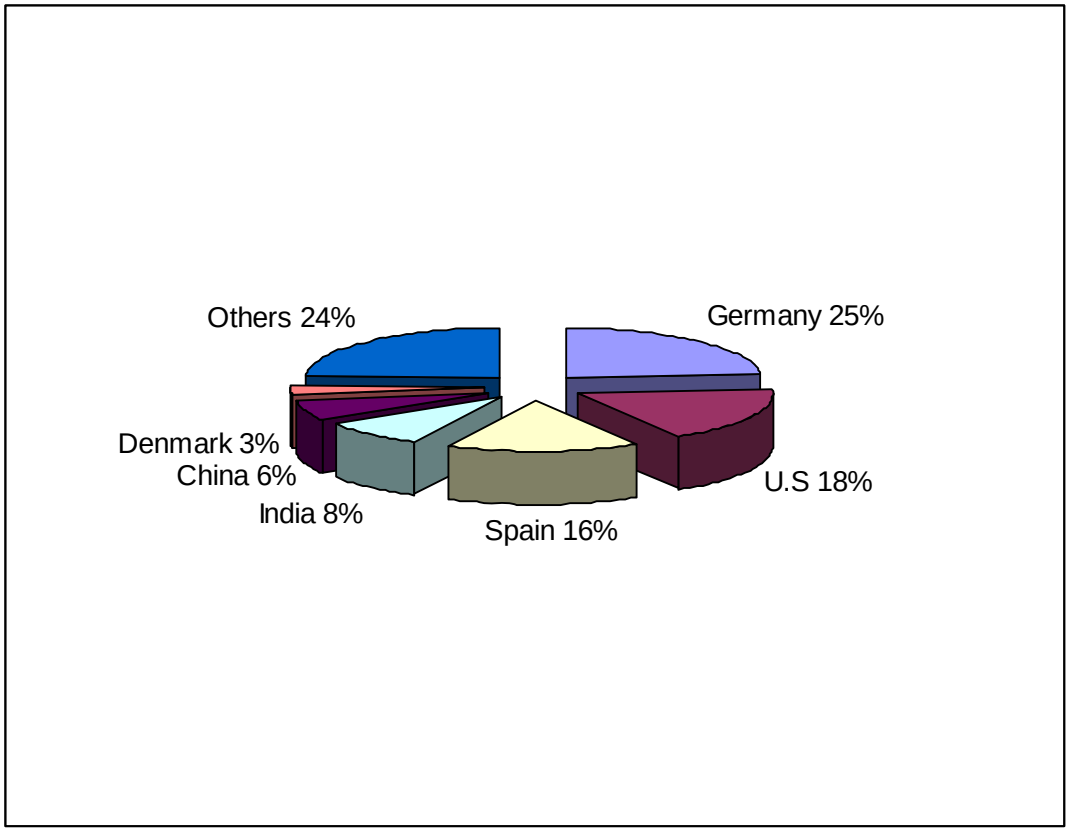

Figure 1.5: Top cumulative installed wind power capacity by percentage (World, 1980-2007)

Statistics have also shown that in the year 2007, in North America, the total installed capacity increased its share of the worldwide market of wind power. The U. S. is further concentrating and developing other sites, apart from the two states of California and Texas, which together accounted for about two thirds of the national total of 4,660 MW. The Canadian Wind Energy Association, CANWEA, disclosed the total installed capacity for wind energy in 2007 at 1,846 MW. A total

of about 560,000 homes now derive their electricity needs from wind power. Canada, with one of the largest wind resources in the world, has a large potential to expand its wind energy market. In 2004, only a total of 444 MW had been reached [8].

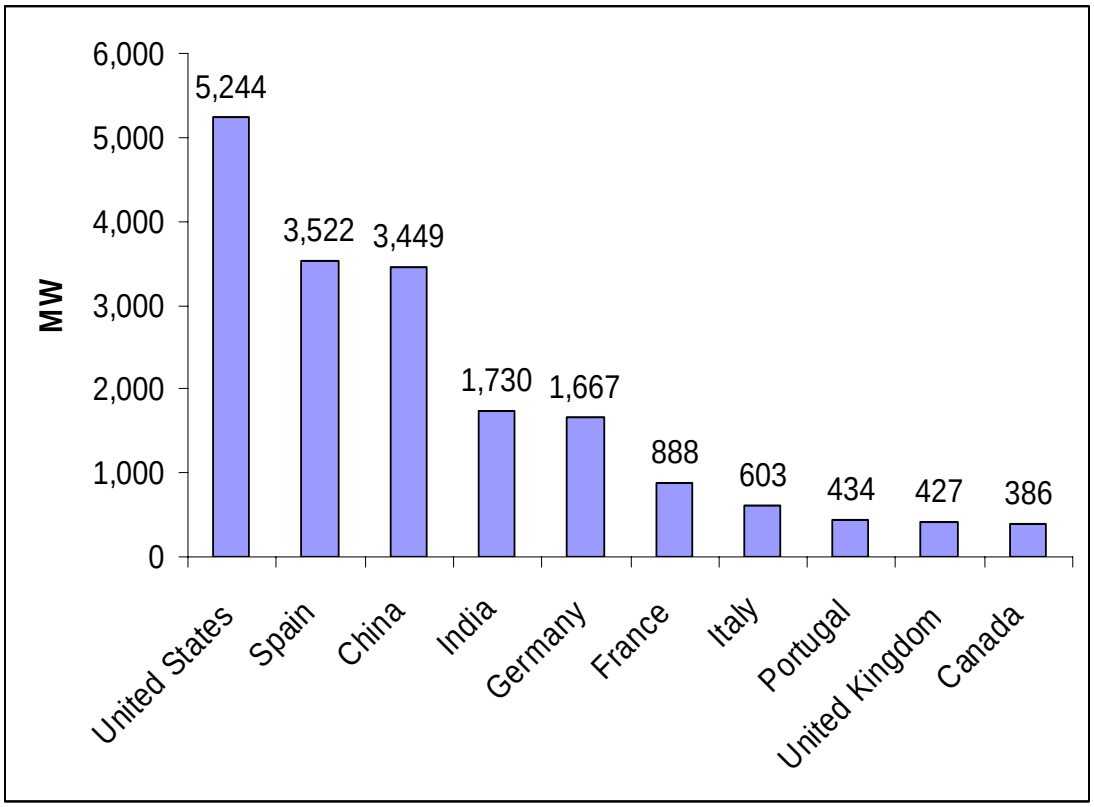

Figure 1.6: Wind power capacity in 2007: Top 10 countries [4]

The North American market experienced the greatest growth worldwide in 2007, with 5,244 MW of new energy capacity built in the United States alone. Germany, the leader in Europe cumulatively, experienced a decline, while Spain has taken the leadership in installed capacity. Canada is currently the world's 11th

ranked nation for installed wind energy capacity. Given the huge potential of its wind resources, the Canadian government believes wind energy is an important component of its strategy to addressing climate change [8]. There is also growing research into enhancing the wind power development. Zephyr Alternative Power, in collaboration with the University of Ontario Institute of Technology, is developing a novel Zephyr vertical axis wind turbine. This joint effort aims to improve upon the existing power output from the turbine. This collaboration and turbine development can contribute to the overall growth of wind in urban areas.

1.3 Wind Turbine Technology

Many different wind generators have evolved over the years. Whatever form the alterations in design have taken, they normally fall into two basic classifications: horizontal axis wind turbine (HAWT) and vertical axis wind turbine (VAWT). Rotors that spin about a horizontal axis are called HAWT and those whose rotors spin about a vertical axis are VAWT. The vertical axis wind turbines are further grouped into two types: the drag–based devices that use aerodynamic drag to extract power from the wind, and lift–based types (note: lift refers here to the force acting perpendicular to the blade)

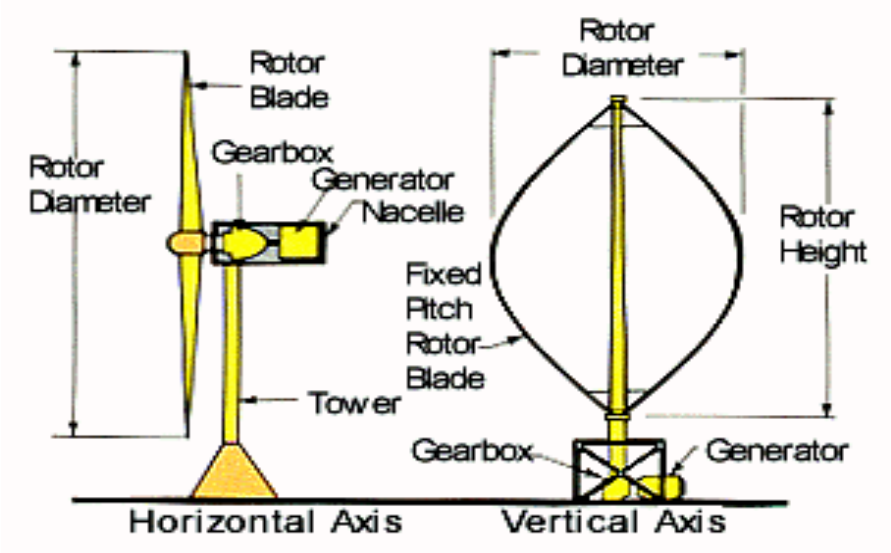

Figure 1.7: Wind turbine types

(Source: American Wind Energy Association) www.awea.org

The turbine industry today is dominated by the conventional horizontal axis wind machines. The vertical axis wind turbines (VAWTs) are uncommon. Unlike VAWTs, the horizontal wind turbines are not omni-directional. As the wind direction changes, HAWTs must also change direction to continue functioning. There must be a technique for orienting the rotor with respect to the wind. In a HAWT, the generator directly converts the wind energy, which is extracted from the rotor. The rotor speed and power output can be controlled by pitching the rotor blades along the longitudinal axis. A mechanical or electronic blade pitch control mechanism can be used, in order to control the pitch angle. An important advantage of a HAWT is that blade pitching can also protect against extreme wind conditions

and speed. Also, the rotor blades can be shaped to achieve maximum turbine efficiency, by exploiting the aerodynamic lift to a maximum.

The advantages of VAWTs are they can accept wind from any direction, thus eliminating the need for re-orienting towards the wind. This simplifies their design, reduces cost of construction, aids installation, and eliminates the problem imposed by gyroscopic forces on the rotor of a conventional machine, as the turbine tracks the wind. The vertical axis of rotation also permits mounting the generator and drivetrain at ground level. However, a shortcoming is it is quite difficult to control power output by pitching the rotor blades, as they are not self-starting and they have a low tip-speed ratio [7]. Nevertheless, the VAWT is attracting a growing interest globally. Its modular and scalable size, among other advantages over conventional HAWTs, is attracting researchers and developers who are working to improve and optimize this type of turbine.

1.4 Thesis Objectives

Following the oil crisis and consequent energy problems of the 1970s, wind turbine technology has witnessed a rapid development, amidst an urgent requirement for sustainable alternatives to the continuous rising cost of fossil fuels. Global warming will continue unless dependence on fossil is reduced. Wind power has a key role in reducing greenhouse gas emissions. The Zephyr turbine is a promising type of wind turbine that can be installed in urban area, where popular

HAWTs have limited capabilities. The Zephyr vertical axis wind turbine (ZVWT) is a novel wind turbine that is capable of producing electric power for homes and industries. The objective of this thesis is to conduct an investigation of ZVWT model geometry modifications with CFD simulations. The performance characteristics will be predicted. Non-dimensional relations for the efficiency of two basic configurations will be obtained. Through these CFD simulations and resulting non-dimensional power curves, new design tools will be developed to improve the performance and operating capabilities of the Zephyr vertical axis wind turbine.

Chapter 2

VERTICAL AXIS WIND TURBINE

HAWTs and VAWTs are both wind power generators that convert kinetic energy of the wind into electric power. A major disadvantage with the HAWTs is power generation ability lost when the wind speed exceeds a certain value known as the cut-off speed. Shutting down is required due to safety and protection of the wind turbine structures, mainly blades during high wind speed. Most HAWTs have a rotor cut-off speed range from 20 to 25 m/s. HAWTs are therefore not suitable in cyclone and storm prone areas. Also, they are not suitable in urban areas. The VAWT has several advantages over HAWTs, such as suitability in urban areas, low noise at low tip speed ratios, better esthetics to integrate into architectural structures, insensitivity to yaw wind direction and increased power output in skewed flow [7, 9]. These advantages have led to a growing research interest in VAWTs, to bridge the gap of shortcomings with HAWTs. New advances in VAWTs and the Zephyr wind turbine design will be the focus of this thesis. The aerodynamic performance of vertical-axis wind turbines and computational simulations will be examined.

2.1 VAWTs Background

The origin of VAWTs can be traced back to roots in Persia [10, 11]. The windmill was used as a source of mechanical power in the tenth century. Inhabitants, who lived in Eastern Persia, utilized the windmills as vertical-axis and

drag type of windmills illustrated in Figure 2.1. The invention of the vertical-axis windmills subsequently spread in the twelfth century throughout the Middle East and beyond to the far East. The basic mechanisms of the primitive vertical-axis windmills were used in later centuries, such as placing the sails above the millstones, elevating the driver to a more open exposure, which improved the output by exposing the rotor to higher wind speeds, and using reeds instead of cloth to provide the working surface [10].

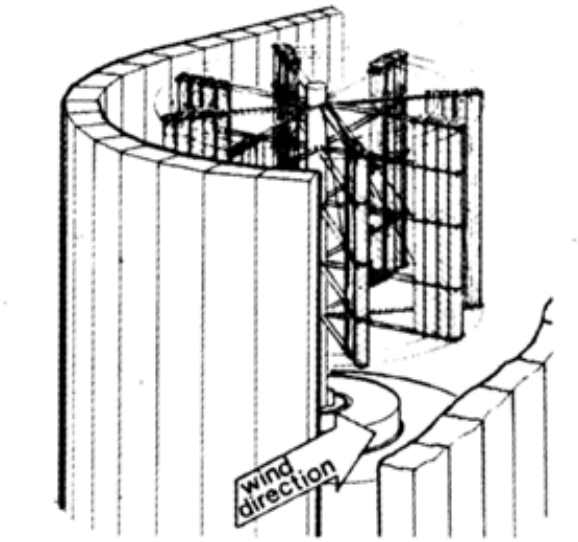

Figure 2.1: Persian windmill [11].

A transition was witnessed from windmills supplying mechanical power, to wind turbines generating electrical power, which occurred toward the end of the nineteenth century. The initial use of wind for electricity generation, as opposed to mechanical power, led to the successful commercial development of small wind

generators, further research and experiments with large turbines. It is also worthy to note that the development of the aircraft industry in the early part of twentieth century facilitated rapid advances in airfoils which could immediately be applied improvement of the wind turbine [10].

Two types of vertical axis wind turbines are commercialized today in the wind energy market: Darrieus and Savonius types. The following section will provide an overview of these turbines.

2.1.1 Darrieus Lift-Based VAWT

Invented by F.M. Darrieus in the 1930s, Darrieus turbines are lift-based turbines designed to function on the aerodynamic principle of airplanes [12]. The rotor blades are designed as an airfoil in cross section, so the wind travels a longer distance on one side (convex) than the other side (concave). As a result, the wind speed is relatively higher on the convex side. If Bernoulli's equation is applied, it can be shown that the differential in wind speed over the airfoil creates a differential pressure, which is used to pull the rotor blade around as the wind passes through the turbine. The Darrieus VAWT is primarily a lift-based machine, which is a feature that makes it compete in performance with the conventional HAWTs. Figure 2.2 shows a typical Darrieus wind turbine characterized by its C-shaped rotor. It is normally built with two or three rotor blades. It has a low starting torque, but high rotational speed, making it suitable for coupling with an electrical

synchronous generator. For a given rotor size, weight and cost, its power output is higher than any drag-based VAWT [10]. But the Darrieus VAWT suffers a disadvantage by not self-starting. Experimental studies of Savonius – Darrieus wind turbines have been conducted [11]. The result of the combined designs shows an improvement in power generation efficiency. The high starting torque of the drag Savonius turbine type is an advantage to starting the Darrieus machine under a hybrid system.

Figure 2.2: Darrieus wind turbine [5]

Darrieus turbines are well known vertical axis wind turbines with unique curved blades, which remove the centrifugal force on the blades. They have several advantages in comparison with conventional, propeller-type, horizontal axis wind turbines [10]. The maximum power coefficient can be obtained at a lower TSR,

compared to conventional wind turbines. Flow induced noise is therefore less than noise from conventional turbines. Although the VAWT has high performance and advantages in comparison with conventional wind turbines, the operations of VAWTs in general are still limited to locations in parks, buildings, monuments or other architectural structures in urban or rural areas.

2.1.2 Savonius-Drag Based VAWT

Savonius wind turbines are drag based VAWTs that operate on the theory and principle of a paddle propelling a boat through water. It was invented by a Finnish engineer, S.J. Savonius. If no slip exists between the paddle and water, the maximum speed attained will be the same as the tangential speed of the paddle. Similarly, in a drag based VAWT, the speed at the tip of the blade can seldom exceed the speed of the wind. In order words, the drag can also be described as the pressure force or the thrust on the blades created by the wind as it passes through it.

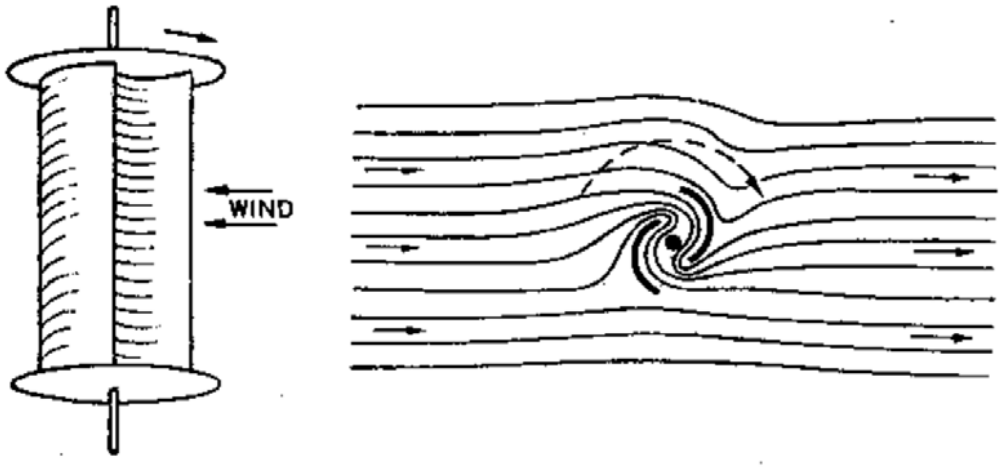

Figure 2.3: Savonius rotor [27]

Various types of drag based VAWTs have been developed in the past which use plates, cups, buckets, oil drums, etc. as the drag device. The Savonius rotor is an S - shaped cross section rotor (see fig. 2.2), which is predominantly drag based, but also uses a certain amount of aerodynamic lift. Drag based VAWTs have relatively higher starting torque and less rotational speed than their lift based counterparts. Furthermore, their power output to weight ratio is also less [7, 10]. Because of the low speed, these are generally considered unsuitable for producing electricity, although it is possible by selecting proper gear trains. Drag based windmills are useful for other applications such as grinding grain, pumping water and a small output of electricity. A major advantage of drag based VAWTs lies in their self–starting capacity, unlike the Darrieus lift–based vertical axis wind turbines.

2.2 Recent Developments in Modern Savonius Turbines

A major disadvantage of the lift based Darrieus VAWT is its weak self-starting capability. In the case of a low TSR, the average torque of the turbine is almost zero or sometimes negative. Therefore, starting motors or engines are required. The other problem of this VAWT is a small effective operation range. Although the maximum power coefficient of the Darrieus VAWT is of the same order of magnitude as a conventional turbine, the effective TSR operation range is too narrow for electric power generators. This disadvantage reduces the net amount of electricity generation from the VAWTs. The Savonius wind generators have

therefore attracted growing interest, due to their high starting torque, among other reasons.

Developments in other related areas of wind technology have been adapted to the drag based wind turbine, which will help improve its presence in the global wind market. Some related fields that have contributed to a new generation of wind turbines include material science, computer science, aerodynamics, analytical methods, testing and performance estimation [10, 13]. Material science developments have brought new composites for blades and alloys in the metal components. Developments in computer science and CFD codes have facilitated new design, analysis, monitoring and control. Aerodynamic design methods, originally developed for the aerospace industry, have been extended to wind turbine development. Analytical methods have been developed to a stage where it is possible to have much better understanding of how a new design should perform. Testing with a vast array of commercially available sensors, coding, data collection and analysis equipment allows designers to better understand how the new turbines actually perform.

Savonius turbine studies have shown efficiencies that can reach up to 37%. Sorensen and Newman [19, 23] have conducted experiments to investigate the effects of geometrical parameters, such as blade gap size, number and overlap. Computational simulation software is a useful design tool to improve the turbine performance.

Computational Fluid Dynamics is an important tool for the analysis, development, and optimization of wind power systems. Various CFD techniques have been used to simulate turbine performance, such as the viscous three-dimensional differential/actuator disk method, adapted by Ammara, Leclerc and Masson [14] for the aerodynamic analysis of wind farms. In order to improve VAWT performance, CFD can be used to predict flow fields around a VAWT. The flow field around a VAWT is complicated, because of interactions between the large separated flow and wake itself. The flow field through a VAWT is essentially unsteady, turbulent and separated flow. Akiyoshi et al. [13] simulated flow around a VAWT and estimated its aerodynamic performance. The sub-grid scale turbulence model was developed to simulate the separated flow from the turbine blades. A sliding mesh technique was introduced to simulate flow through the rotational blades. Numerical results were compared with predictions based on momentum theory.

Computer simulations of the Navier-Stokes equations have been applied to solve wind turbine problems. Blade Element Momentum (BEM) theory is a common theoretical method developed for blade optimisation and rotor design [15, 16, 17]. With Computational Fluid Dynamics (CFD), Navier–Stokes equations are solved together with models approximating turbulence to reveal the flow characteristics. The results of such modelling are useful, providing large amounts of data detailing the flow pattern. The difficulty of using such method is in computing time, particularly when high resolution is needed near the blades [16]. Therefore,

when the flow pattern near the blades is modeled, theoretical methods can be used to simplify this procedure. Numerical analyses have been carried out to investigate the flow fields behind a small wind turbine with a flanged diffuser [15]. Wang et al. [16] have used a scoop design with CFD as a tool for improving the turbine wind energy capture, under low wind speed. These studies seek to enhance the wind speed across the turbine rotor, which will be installed in built up cities. In this thesis, the stator veins of the Zephyr turbine will be tested to improve their performance. Similar past studies [16, 18] used a representation of the rotor using a disk loading technique. Mandas et al. [20] modeled a three-dimensional large-scale wind turbine using Fluent, and they compared the results with those obtained from the BEM theory. In predicting the power characteristics of the Zephyr vertical axis wind turbine, CFD can also be used as a modelling tool. Power output is the key variable to be examined in this thesis by CFD modeling. A finite volume technique will be used to analyze the performance of a two-dimensional vertical axis wind turbine. Rajagopalan [33] developed a finite volume method to predict drag characteristics of turbine blades.

CFD numerical techniques are useful in various flow aspects of turbine performance. The viscous three-dimensional differential/actuator disk method has been used for the aerodynamic analysis of wind turbine. In this approach, the rotor is modeled as a permeable surface from which the time-averaged mechanical work is extracted by the rotor from the air.

A common method for modeling the rotation of a turbine blade is the steady-state multiple reference frame model. This method was applied by Hahm and Kröning [21] to study the wake effects of horizontal wind turbines. The method was also utilized by Fluent Inc. to simulate a three rotor horizontal axis wind turbine (HAWT) at the National Wind Technology Center (NWTC). The computed generator power and operating efficiency predicted by Fluent was within 1% of the collected field data [22]. A more computationally demanding CFD method is the moving mesh model. Sezer-Uzol and Long [23] developed a three-dimensional time-accurate simulation of HAWT rotor flow fields. Results shown good agreement exist between the simulated pressure coefficient distributions and experimental data was achieved by the authors.

The torque and pressure on the rotors of a vertical axis wind turbine (VAWT) are important parameters for a design. With many VAWTs, especially designs with high rotor-stator interaction, the power output of the turbine can be rapidly changing and diverse throughout each rotation. For such applications, an unsteady time-dependant CFD simulation can offer a useful and straightforward method for determining a turbine's power output throughout each cycle. This technique is effective even for power curves with a high level of fluctuation. This is an important benefit of the moving mesh model, as it is the only method available to produce reliable time-dependent results.

The MRF model is another alternative for obtaining transient flow information [28]. With most VAWTs, the torque on each rotor varies significantly throughout each cycle. Plotting the torque through a full rotation can provide the designer with useful information about material fatigue, cyclic stresses, maximum torque, turbine performance, and possible areas of efficiency improvements. The MRF model also has useful applications for the analysis of VAWTs. Important data for the understanding and optimized use of a wind turbine lies in the characteristic power curve (power vs. rotational velocity and power vs. wind velocity). Attempts have been made to develop effective, accurate and simplified methods to determine a VAWT's characteristic power curve. Camporeale, Fortunato and Marilli [24] developed an automatic system that is automated and able to determine a larger number of data points than a traditional system using variable resistors. A CFD simulation can provide a useful alternative for estimating a turbine's characteristic power curve, with virtually any number of data points. In this thesis, CFD will be used to predict the velocity and pressure distributions for a novel Zephyr VAWT, from which design modifications will be made to improve the turbine's performance.

2.3 Zephyr VAWT.

The Zephyr VAWT is a Canadian invented wind generator. It is a special drag based turbine with lift to boost its power output. The modular and scalable design is quiet; visually appealing and practical for residences and institutions (see fig. 2.4). This thesis aims to improve upon the current design, which has the

capability of harnessing up to 20% more wind energy than a HAWT [34]. To significantly increase the blade's rotor speed and energy efficiency, the effects of geometric modification on this improved performance are considered in this thesis. Curved blades have been found to be more efficient than either the twisted or straight blade types [26]. The ZVWT special features of the stationary vein angles, pressure zones, rotary blades, angle and spacing will be optimized. Few if any studies have examined this type of flow distribution through a VAWT with CFD, due to the unique complexity of its geometry and dynamics in comparison with a HAWT. Through advances in computer hardware, CFD with personal computers have becomes an empowering tool to make these simulations economically viable. It is Zephyr's goal to develop and market these small to medium size installations (up to 50 kW) internationally.

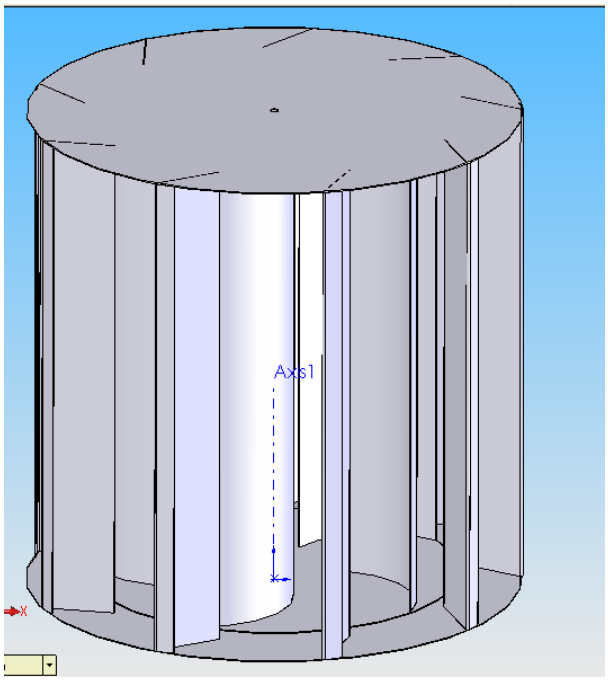

Figure 2.4: Zephyr VAWT.

Figure 2.5: PacWind VAWT. www.pacwind.net

PacWind is a U.S. based developer of a PacWind VAWT. This turbine (see fig. 2.5) has a performance capability yielding a power output of 1.0 KW during a favorable wind speed. It measures 55 inches (1.40metres) high by 30 inches (0.76metres) in diameter. The power curve for the PacWind, based on CFD simulation data made available is plotted in the result section of this thesis. The result show this turbine doesn't start produce reasonable power until the wind speed reaches 25 MPH (11 m/s), with the rated capacity reached at about 43 MPH (20 m/s). The Zephyr VAWT is unique with its stator veins, which favor a much lower wind speed. Unlike the PacWind VAWT, it measures 30 inches (0.76 metres) height by 30 inches (0.76 metres) wide. The ZVWT's unique features allow it to perform in both low wind and high turbulence conditions.

Chapter 3

AERODYNAMICS AND PERFORMANCE MODELS

Achieving success in harvesting the power of wind requires a detailed understanding of the physics of the interaction between the moving air and wind turbine rotor blades. An optimum power production depends on perfect interaction. The wind consists of a combination of the mean flow and turbulent fluctuations about that mean flow. In this chapter, the basic prevailing aerodynamic phenomena for the VAWT will be highlighted. Aerodynamic forces caused by wind shear, off-axis winds, rotor rotation, randomly fluctuating forces induced by turbulence and dynamic effects all affect the fatigue loads experience by a wind turbine. These are very complicated for the VAWT, and they can only be predicted by understanding the aerodynamics of steady state operation. An idealized wind turbine rotor will be examined along with the airflow around the generator rotor. An analysis to determine the theoretical performance limits for wind turbines by a blade-element theory will be developed. Also, a CFD computational solution for the aerodynamic design of a wind turbine rotor will be performed.

3.1 Aerodynamics Theory and Performance Characteristics

The aerodynamic analysis of VAWTs is complicated due to their orientation in the oncoming wind. The VAWTs have a rotational axis perpendicular to the oncoming airflow. This accounts for aerodynamics that is more complicated than a conventional HAWT. However, the configuration has an independence of wind direction. The main shortfalls are the high local angles of attack and the wake

coming from the blades in the upwind part and axis. This disadvantage is more pronounced with Savonius (pure drag) VAWTs, when compared to the Darrieus VAWTs. The power output from the high speed lift VAWT can be appreciable. Understanding the aerodynamics of the pure drag type of VAWT will give important insight for improving the lift coefficient, and designing this turbine for better and more efficient harnessing of the wind energy.

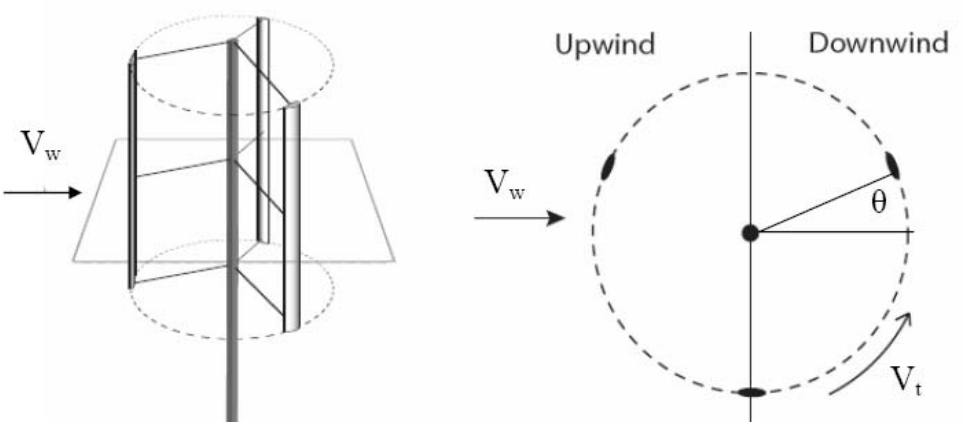

(a) 3-D (b) 2-D cross section

Figure 3.1: VAWT model. [20]

Figure 3.1 shows a typical VAWT model in both three and two dimensional orientations.

3.2.1 Lift Force

The lift force, L, is one of the major force components exerted on an airfoil section inserted in a moving fluid. It acts normal to the fluid flow direction. This

force is a consequence of the uneven pressure distribution between the upper and lower blade surfaces (see fig. 3.2), and can be expressed as follows:

$$L = 0.5 C_l \rho V^2 A \tag{3.1}$$

where ρ is the air density, C_l is the lift coefficient and A is the blade airfoil area.

3.2.2 Drag force

The drag force, D acts in the direction of the fluid flow. Drag occurs due to the viscous friction forces on the airfoil surfaces, and the unequal pressure on surfaces of the airfoil. Drag is a function of the relative wind velocity at the rotor surface, which is the difference between the wind speed and the speed of the surface, and can be expressed as

$$D = 0.5 C_d \rho (U - \Omega r)^2 A \tag{3.2}$$

where Ωr is the speed of the surface at the blade, C_d is drag coefficient and V is the wind speed.

The lift and drag coefficient values are usually obtained experimentally and correlated against the Reynolds number. In this thesis, a CFD code will be used to predict these coefficient values over a range of operating conditions. The amount of power generated by the novel Zephyr vertical axis wind turbine will be analyzed. A

section of a blade at radius *r* is illustrated in Fig. 3.2, with the associated velocities, forces and angles shown. The relative wind vector at radius *r*, denoted by V_{rel}, and the angle of the relative wind speed to the plane of rotation, by ϕ. The resultant lift and drag forces are represented by *L* and *D*, which are directed perpendicular and parallel to the relative wind as shown

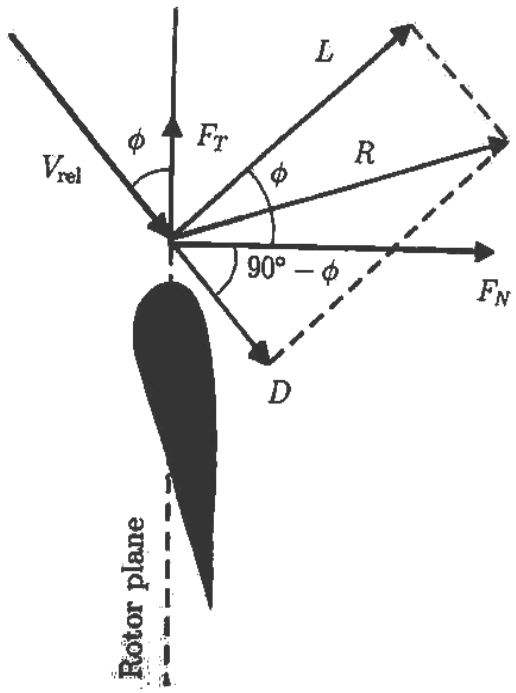

Figure 3.2: Local forces on a blade [10]

A careful choice of the rotor blades geometry and shape modification is crucial for maximum efficiency. Wind turbines have typically used airfoils based on the wings of airplanes, although new airfoils are specially designed for use on rotors. Airfoils use the concept of lift, as opposed to drag, to harness the wind's energy. Blades that operate with lift (forces perpendicular to the direction of flow)

are more efficient than a drag machine. Certain curved and rounded shapes have resulted most efficient in employing lift. Improvements of the lift coefficient for the Zephyr turbine depend on geometry, to enhance the performance.

When the edge of the airfoil is angled slightly out of the direction of the wind, the air moves more quickly on the downstream (upper) side creating a low pressure. On the upstream side of airfoil, the pressure is high. Essentially, this pressure differential lifts the airfoil upward. (see Fig. 3.3). In the case of a wind turbine, the lift creates a turning effect. An operating condition with a low blade angle of attack, α, thus favors lift force. An optimum design configuration of Zephyr turbine can reduce the high blade angle of attack responsible for VAWTs dominant drag.

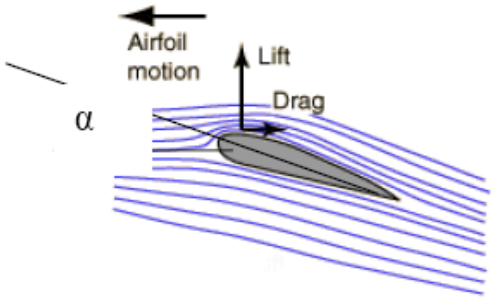

Figure-3.3 Airflow around an airfoil [32].

Bernoulli's principle indicates how faster flow implies lower pressure on the airfoil:

$$P + \frac{1}{2}\rho v = \text{constant} \tag{3.3}$$

The first term in equation. (3.3) is the static pressure and the second term is the dynamic pressure. An increase in velocity leads to a corresponding decrease in the static pressure to maintain a constant, and vice versa. The equation can be understood through a conservation of energy as pressure work is converted to / from kinetic energy in the flow field.

3.2.3 Reynolds number

The Reynolds number Re is the ratio of the inertia forces to the viscous forces. It is a non-dimensional parameter that defines the characteristics of the fluid flow conditions. It is used when calibrating the lift and drag coefficients of an airfoil. For a high speed rotor,

$$\mathrm{Re} = \frac{UL}{v} = \frac{\rho UL}{\mu} = \frac{\rho V_\theta c}{\mu} \quad , \tag{3.3}$$

where μ is the fluid viscosity, $v = \frac{\rho}{\mu}$ is the kinematics viscosity, L is the characteristics length scale, c is the blade chord length, and V_θ is the blade tip velocity

3.2.4 Blade Solidity

The blade solidity, δ, is the ratio of the blade area compared with the swept area. For a vertical axis wind turbine, the solidity is defined as

$$\delta = \frac{Bc}{2\pi r} \tag{3.4}$$

where B is the number of blades. Changing the number of blades or the blade chord dimensions will alter the VAWT solidity. An increase in the chord results in a large aerodynamics force and consequently in high power.

3.2.5 Tip speed ratio

The tip speed ratio λ, is defined as the velocity at the tip of the blade, to the free stream velocity. The rotational speed can be varied by the turbine controller for a certain wind speed. The rotational speed, ω, is therefore represented by the tip speed ratio, λ. This parameter gives the tip speed, $R\omega$, as a factor of the free stream velocity, V. It is given by

$$\lambda = \frac{R\omega}{V} \tag{3.5}$$

3.2.6 Bezt number

The Bezt number or Bezt limit is a useful performance indicator of wind turbines. It is the maximum amount of power that can be extracted by a wind generator from the available wind kinetic energy. This maximum turbine power is the difference between the upstream and downstream wind powers (see fig. 3.1b).

$$P_t = \frac{1}{2} * \frac{dm}{dt} * (V^2 - V_0^2) \tag{3.6}$$

where P_t = turbine output power (watts),

V = upstream wind velocity (m/s) and

V_0 = downstream wind velocity (m/s)

The mass of air flowing through the turbine rotor area is a function of the air density and velocity (upstream and downstream average),

$$\frac{dm}{dt} = \rho_{air} A * \frac{1}{2}(V + V_0) \tag{3.7}$$

Substituting equation (3.7) into equation (3.6), the turbine power becomes

$$P_t = \frac{1}{2}\left[\rho_{air} * A * \frac{(V + V_0)}{2} \right] * \{V^2 - V_0^2\} \tag{3.8}$$

Equation (3.8) is rearranged to give the following expression:

$$P_t = \frac{1}{2} * \rho_{air} * A * V^3 * \frac{\left(1 + \frac{V_0}{V}\right) * \left[1 - \left(\frac{V_0}{V}\right)^2\right]}{2} \tag{3.9}$$

This power from the turbine rotor can be expressed as a fraction of the upstream wind power, i.e.,

$$P_t = \frac{1}{2} * \rho_{air} * A * V^3 * C_p \tag{3.10}$$

where C_p is the fraction of power captured by the rotor blades also called power coefficient or *rotor efficiency*.

Re-arranging the previous results, it can be shown that

$$C_p = \frac{\left(1 + \frac{V_0}{V}\right) * \left[1 - \left(\frac{V_0}{V}\right)^2\right]}{2} \tag{3.11}$$

Figure 3.3 shows the variation of C_p with downstream to upstream wind speed ratio, V_0/V. The theoretical maximum rotor power coefficient is C_p = 16/27 (= 0.59), when the downstream to upstream wind speed ratio is V_0/V = 0.33, called the *Betz*

limit after the first analysis carried out by Betz (1926). However, the practical limits for C_p are typically 0.46 for high speed two-blade system and 0.50 for three-blade turbines. The drag turbine operates at about 1/3 of the 0.59 Bezt limit.

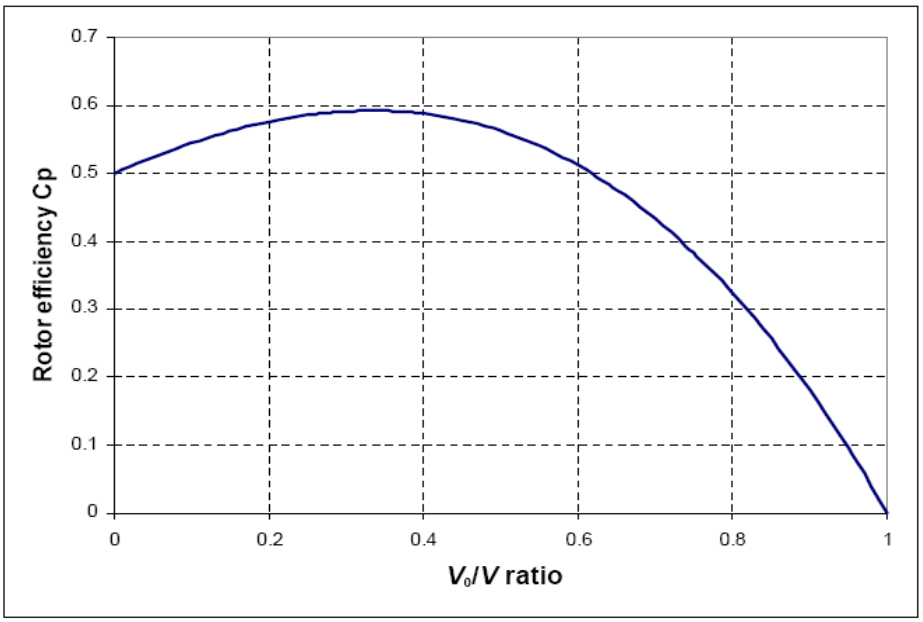

Figure 3.4 - Rotor efficiency vs. downstream / upstream wind speed ratio [26]

As with all turbines, only a part of the energy shown in fig. 3.4 can be extracted. If too much kinetic energy were removed, the exiting air flow would stagnate and thus cause blockage. When the air flow approaches the inlet of the turbine, it meets a blockage imposed by the rotor-stator blades. This causes a decrease in kinetic energy, while the static pressure increases to a maximum at the turbine blade. As the air continues through the turbine, energy in the fluid is transferred to the turbine rotor blades, while the static pressure drops below the atmospheric pressure as fluid flows away from the rotor. This will eventually

further reduce the kinetic energy. Then kinetic energy from the surrounding wind is entrained to bring it back to the original state.

A "disk actuator" model of a HAWT gives further insight into the process. This model can be used in explaining the Bezt limit.

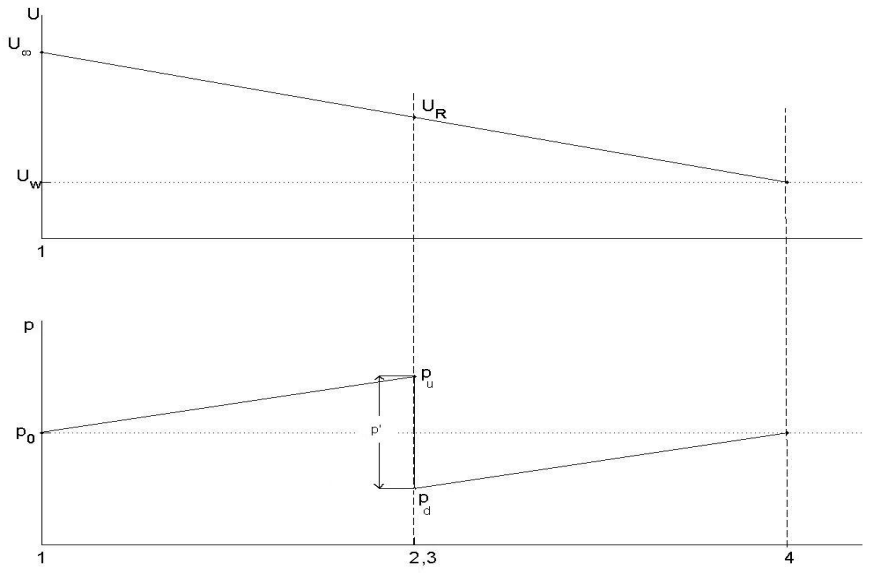

Figure 3.5: Velocity and pressure distribution in a stream tube

Typical velocity and pressure distributions are illustrated in Figure 3.5, using the disk actuator model and Bezt limit theory. If the stream tube model is applied to a VAWT, it gives insight into the velocity and pressure distributions for a Zephyr VAWT. Because of the continuity principle for the stream tube, the diameter of the flow field must experience an increase as the velocity decreases giving rise to a

sudden pressure drop, $\{p' = (p^u - p_d)\}$, at the rotor plane. This pressure drop contributes to the torque for rotating turbine blades.

The actuator disk theory also provides a rational basis for illustrating the flow velocity at the rotor is different than the free-stream velocity. The Betz limit from the actuator disk theory shows the maximum theoretically possible rotor power coefficient (0.59) for a wind turbine. In reality, three major effects account for a power coefficient:

• rotation of wake behind the rotor;

• finite number of blades and associated tip losses;

• non-zero aerodynamic drag.

3.3 Rotor Performance Parameters

A wind turbine designed for a particular application should have its performance characteristics tested before proceeding to prototype fabrication. A dimensionally similar and scaled down prototype of the design model is normally tested in a wind tunnel for this purpose. CFD commercial software is also used to save time and cost [15, 16].

The power performance of a wind turbine is normally expressed in dimensionless form. For a given wind speed, the power coefficient and the tip speed ratio are good indicators to use as a performance measure. For a particular configuration of the Zephyr VAWT, these parameters are

$$C_p = \frac{P_t}{\frac{1}{2}\rho V^3 A} \tag{3.12}$$

where $A = hd$, d is the rotor diameter and h is the height of turbine. Also, C_p and λ (tip speed ratio) of equation 3.5 are dimensionless values used in predicting the performance of the turbine. Figure 3.5 shows typical sample predictions for different wind turbine types. The Zephyr wind turbine is a special type of the Savonius VAWT.

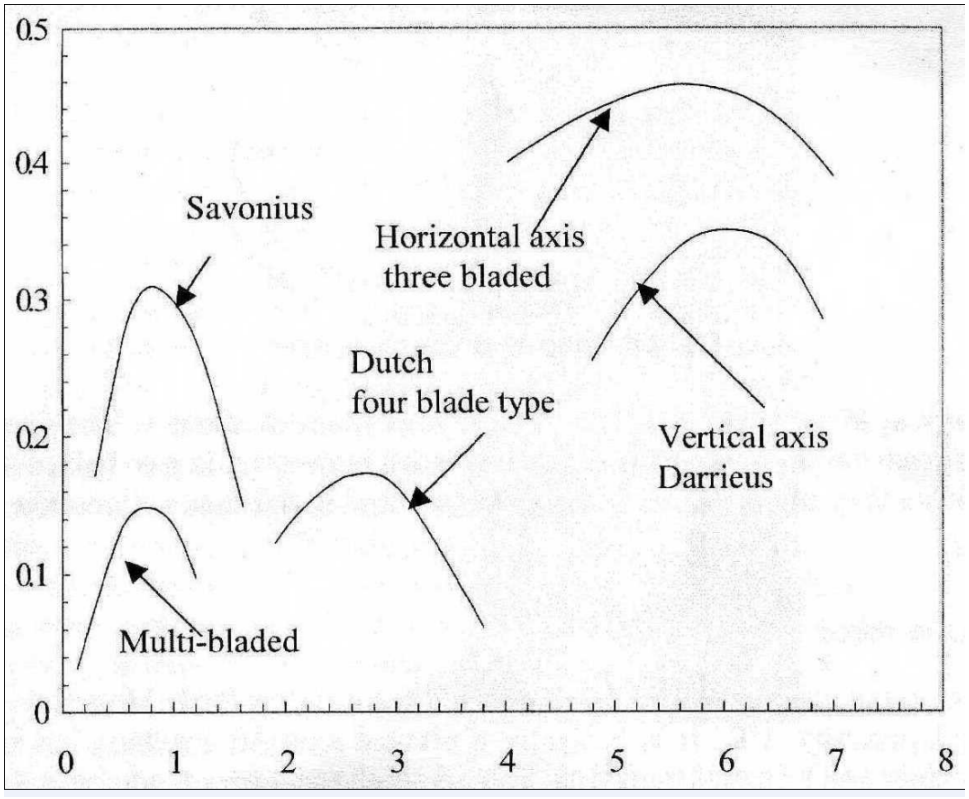

Figure 3.5 - Rotor efficiency vs. tip speed ratio [26]

Figure 3.5 is a sample extract [26]. It is an illustration of modern turbine C_p - λ curves with C_p and λ are represented on the plot as y-axis and x-axis respectively.

3.4 Blade Element Theory

Blade Element Momentum (BEM) theory is a theoretical method developed for blade optimization and rotor design. The Blade Element Momentum theory, otherwise called strip theory, is a combination of basic momentum theory and blade element theory. The motion of the air flow and forces acting on the blades, determined by momentum principles are not complete without examining the shape of blades and configuration required for optimum and improved rotor power performance. The main principle of blade element theory is to consider the forces experienced by the blades of the rotor in motion through the air. This theory is therefore intimately concerned with the geometrical shape of the blade.

BEM theory becomes an essential tool that relates rotor performance to rotor geometry. A particularly important prediction of this theory is the effect of blade number. An assumption in BEM theory is that individual *stream tubes* (the intersection of a stream tube and the surface swept by the blades) can be analyzed independently of the remaining flow, as assumed in blade element theory. Furthermore, an assumption associated with BEM theory is that *spanwise flow* is negligible, meaning that airfoil data taken from two-dimensional tests are acceptable as in blade element theory. Another assumption is that flow conditions

do not vary in the circumferential direction, i.e., axisymmetric flow. With this assumption, the streamtube to be analyzed is a uniform annular ring centered on the axis of revolution, as assumed in general momentum theory.

The multiple-streamtube model is a well established technique for predicting the performance of VAWTs. It is similar in many ways to that used for HAWTs. The objective of the analysis is to simultaneously determine the forces acting on the blades of the turbine by a "blade element analysis" and deceleration of the wind that occurs due to the energy extracted from the air flow by the turbine, through actuator strip theory. As the rotor of the VAWT revolves, the blades trace the path of a vertical cylinder known as the actuator cylinder. As the wind intersects this cylinder, it must slow and any given streamtube of rectangular cross section must expand horizontally as shown schematically in Figure 3.6

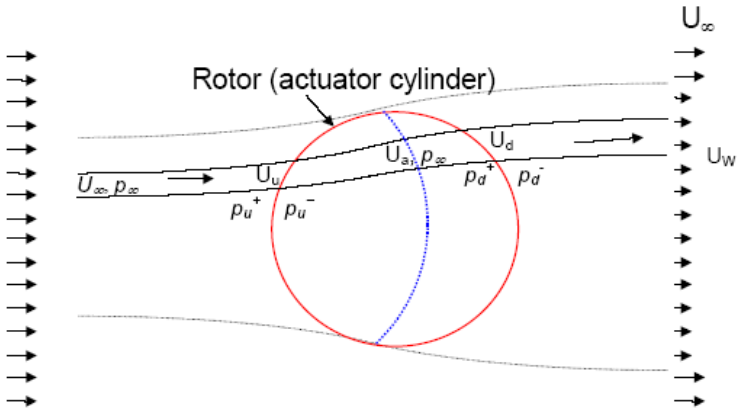

Figure 3.6: Plan view of actuator cylinder to analyse VAWTs [27]

The wind turbine blade performance is determined with BEM by combining the equations of general momentum theory and blade element theory.

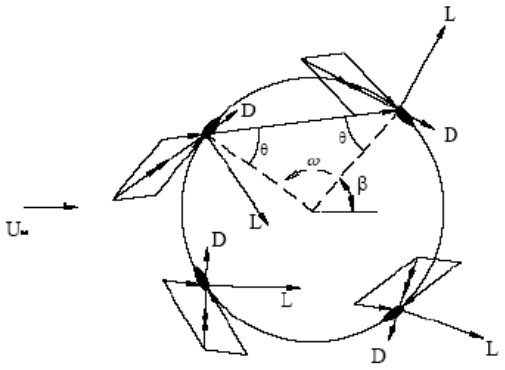

Figure 3.7 lift and drag force on VAWT [27]

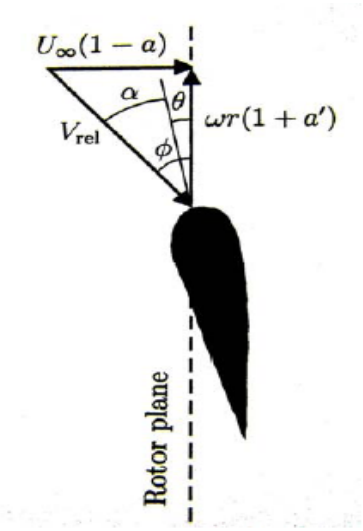

Figure 3.8: Velocities at the rotor plane [10]

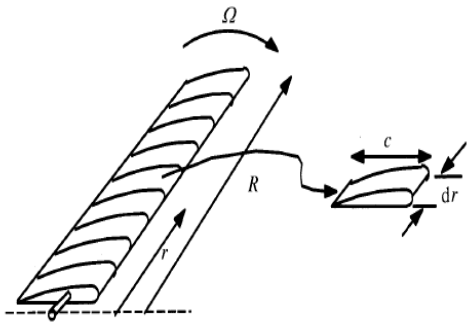

Figure 3.9a: Schematic of blade elements

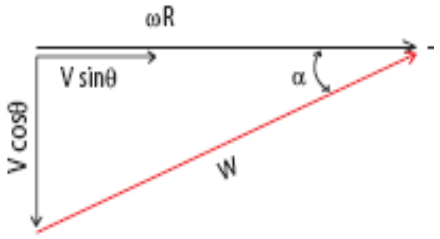

Figure 3.9: Component of local angle of attack

Figures 3.7 and 3.8 show that lift and drag forces, L and D, respectively, could be determined and hence the torque, power output from the blades and mechanical efficiency of the rotor could be determined. Here the symbol β represents the blade azimuth angle, φ is the angle between the resultant wind velocity, V, and the blade velocity (ωr), α is the angle of attack, γ is the blade pitch angle and θ is the angle between the streamtube and the rotor radius. The relative wind velocity V_{rel}, (W) is the vector sum of the wind velocity at the rotor $V_\infty(1-a)$

(vector sum of the free-stream wind velocity, V_∞ and the induced axial velocity - aV_∞) and the wind velocity due to rotation of the blade. The rotational component is the sum of the velocity due to the blades motion, (ωr), and the swirl velocity of the air, a' (ωr) . The axial velocity V_∞ (1- a), is reduced by a component V_∞ a, due to the wake effect or retardation imposed by the blades, where V_∞ is the upstream undisturbed wind speed. The relative wind velocity is shown on the velocity diagram in Figure 3.8. The minus sign in the term V_∞ (1- a) is due to retardation of flow as the air comes into contact with the rotor. The positive sign in the term $\omega.r(1+a')$ occurs due to the flow of air in the reverse direction of blade rotation, after air particles contact the blades and yields torque. This flow ahead and behind the rotor is not completely axial, as assumed in an ideal case. When the air exerts torque to the rotor, as a reaction, a rotational wake is generated behind the rotor. Depending on the wake length or separation, an energy loss is experienced, which resulted in a reduction of the power coefficient.

3.4.1 Torque and Power

The aerodynamic blade loads are transferred through the rotor and they are converted into torque on the low speed rotor shaft. This is the primary drive train load. The rated torque is calculated for a rated wind speed by an analysis of the forces on the surface of the rotor blades. The torque dependence on wind speed and rotor diameter follows a cubic law. It is inversely proportional to the rotor tip speed.

From the blade element analysis, the lift and drag forces acting over the blades are estimated and integrated over the total blade span, incorporating the velocity terms to obtain the shaft torque and power developed by the turbine. As shown on figs 3.2, 3.7 and 3.8 for wind velocity and the force diagram, the lift and drag forces on an element of the blade will produce a differential torque about the axis of rotation as follows:

$$dQ = dQ_L + dQ_D \tag{3.13}$$

where dQ_L is the lift torque contribution (N-m), dQ_D is the drag torque contribution (N-m) and ϕ is the flow angle.

Resolving the forces acting on the blade into total normal and tangential force components yields

$$dF_N = dF_L \cos\phi + dF_D \sin\phi \tag{3.14}$$

$$dF_T = dF_L \sin\phi - dF_D \cos\phi \tag{3.15}$$

Substituting the lift and drag forces eqs. (3.1) and (3.2) into eqs (3.14) and (3.15), while considering an elemental area instead, yields

$$dF_N = 0.5\rho V_{rel}^2 (C_L \cos\phi + C_D \sin\phi) c dr \tag{3.16}$$

$$dF_T = 0.5\rho V_{rel}^2 (C_L \sin\phi - C_D \cos\phi) c dr \tag{3.17}$$

The elemental torque that occurs due to forces acting tangentially over the rotor blade, operating at a distance of rotor radius r from the centre, will give

$$dQ = r.dF_T \tag{3.18}$$

$$dQ = 0.5\rho V_{rel}^2 (C_L \sin\phi - C_D \cos\phi) c r dr \tag{3.19}$$

From fig. (3.8), the relative velocity is given as

$$V_{rel} = \frac{U_\infty (1-a)}{\sin\phi} \tag{3.20}$$

For a turbine rotor with a varying number of rotor blades, the solidity is defined as

$$\delta = \frac{Bc}{2\pi r} \tag{3.21}$$

Substituting equations (3.20) and (3.21) into (3.19), the elemental general equation becomes

$$dQ = \delta.\pi\rho.\frac{U_\infty^2.(1-a)^2}{\sin^2\phi}(C_L \sin\phi - C_D \cos\phi) r^2 dr \tag{3.22}$$

The total power contribution from each blade is thus calculated from the above elemental torque contributions. By integrating along the blade length, the total power is obtained.

The elemental power from each blade element in fig. 3.9 is

$$dP = \frac{B}{2\pi}\Omega dQ \tag{3.23}$$

The total power from the turbine rotor becomes

$$P = \frac{B\Omega}{2\pi}.\int_{A_{Rotor}} dQ \tag{3.24}$$

Substituting this into equation (3.12), the power coefficient C_p is becomes

$$C_P = \frac{\sigma \int_{area} dQ}{1/2\rho_{air} V_\infty^3 A} = \frac{\sigma \int_{area} dQ}{1/2\rho_{air} V_\infty^3 hd} \tag{3.25}$$

3.4.2 Single Streamtube Model

This section extends a past model of Templin [20, 33] to a VAWT, using actuator disk and momentum theories. The flow velocity through the turbine is

assumed to be constant. The application of the momentum theorem between two sections shown in fig. 3.1b yields the drag force. This rotor aerodynamic drag is a vectorial sum of the forces on the actuator disk in the streamwise direction.

$$D = \dot{m}(V_1 - V_2) \tag{3.26}$$

The power exchanged to causes the kinetic energy reduction is given as

$$P = \dot{m}(V_1^2 - V_2^2)/2 \tag{3.27}$$

This power can also be written as follows (assuming a constant velocity):

$$P = D.V \tag{3.28}$$

An assumption is made with the following constant velocity through the stream-tube:

$$V = (V_1 + V_2)/2 \tag{3.29}$$

From blade element theory, the aerodynamic drag force is determined by integrating the forces projected in the flow direction as follows:

$$D = \frac{B}{2\pi}\int_0^{2\pi} (F_N \cos\theta + F_T \sin\theta) d\theta \tag{3.30}$$

The lift and drag coefficients are two-dimensional aerofoil characteristics of the local blade element, which are functions of the angle of attack. They can also be resolved into normal force and thrust coefficients, C_N and C_T, respectively as follows:

$$C_N = C_L \cos\alpha + C_d \sin\alpha \tag{3.31}$$

$$C_T = C_L \sin\alpha - C_d \cos\alpha \tag{3.32}$$

where

$$F_N = C_N qc \tag{3.33}$$

$$F_T = C_T qc \tag{3.34}$$

The total drag force on the turbine for a given number of blades, over a complete revolution, is

$$D = \frac{Bc}{2\pi}\int_0^{2\pi} \{(C_l \cos\alpha + C_d \sin\alpha)\cos\theta + (C_l \sin\alpha - C_d \cos\alpha)\sin\theta\} q d\theta \tag{3.35}$$

From fig. 3.9b, the local angle of attack is

$$\alpha = \arctan\left(\frac{\cos\theta}{\frac{R\omega}{V} - \sin\theta}\right) \tag{3.27}$$

From equation (3.28), the average power will then be

$$P = \frac{Bc}{2\pi} V \int_0^{2\pi} q\{(C_l \cos\alpha + C_d \sin\alpha)\cos\theta + (C_l \sin\alpha - C_d \cos\alpha)\sin\theta\} d\theta \tag{3.36}$$

Equation (3.36) can be solved numerically, given the rotor blade chord dimension and number of blades. It must be ensured that the blade solidity is kept constant. The power obtained is the shaft power, when no load is placed on the turbine. At this stage the mechanical efficiency of the turbine is determined. Then momentum theory can be used to find the dimensionless power coefficient.

3.6 CFD Models

Either CFD or Vortex models are useful alternatives to momentum based theory for predicting wind turbine performance. Unlike the momentum based theoretical model, the vortex and CFD models are capable of predicting behavior of the wake structure near the turbine rotor blades. This arises because the velocity normal to the air flow is not neglected, as with the momentum theory. Computational Fluid Dynamics (CFD) can yield more accurate flow patterns than the momentum and vortex based models. Another advantage is that unsteady flow

calculations can be performed with CFD. Complete flow patterns around 3-D wind turbine can be calculated. The accuracy of the results depends on the mesh spacing and computational model. In the next chapter, this CFD model capability and procedure in optimizing the geometry parameters, as well as predicting the power output of the novel Zephyr vertical axis wind turbine will be outlined.

Chapter 4

Numerical Simulations

4.1 Introduction

After a wind turbine rotor is designed for a specific application, its performance characteristics should be tested before a prototype is fabricated. Often, a dimensionally similar scaled down model of the proposed design are tested in a wind tunnel for this purpose. In this chapter, the capability of CFD commercial software in modeling and simulating an optimum geometry configuration for Zephyr turbine efficient performance is exploited. Numerical simulations of air flow through the Zephyr wind turbine is carried out in this chapter. The mesh discretization and computational model will be described for air flow through the wind turbine. CFD will be used to predict and optimize the geometric parameters, fluid flow and the power output of the novel Zephyr vertical axis wind turbine. The numerical predictions will use a multiple rotating reference frame (MRF) formulation to simulate the turbine performance. The formulation divides the domain into two sub-domains. For the stator and surrounding domain, a stationary reference frame will be used. The rotor reference frame rotates with respect to the inertial frame. It provides a convenient and effective method to investigate the characteristic power curves for the turbine. These power curves are an important element for subsequent development, as they provide estimates of operating

velocities, C_p and TSR. For these simulations, the overall domain will be discretized into quadrilateral-triangular elements due to geometry shape.

4.2 Computational Methodology and Zephyr VAWT design

Small wind turbines such as the Zephyr VAWT are usually assessed by three key parameters: safety/functionality, durability and power characteristics. The power performance among these has a more significant role in guiding the aerodynamic design. Wind turbine power performance before the advent of computers was normally measured in two ways: measure data on a real site, or testing in a wind tunnel. Field monitoring can provide more realistic results, but it needs complicated and robust instrumentation. Furthermore, it takes a longer period to cover various wind conditions so it becomes more expensive than wind tunnel tests. Wind tunnel tests also have some drawbacks; there are limitations on the size of the wind turbine that is tested inside a tunnel. To minimize the effects of obstruction of airflow inside the tunnel, the wind turbine needs to be small enough to ensure that its flow blockage is negligible. Wind turbines are scaled down to fit into the wind tunnel, before testing can take place. Results of such experiments are later extrapolated to larger size by appropriate scaling laws.

Computational Fluid Dynamics (CFD) with commercial Fluent software will be used in this thesis. This will provide a useful wind turbine modeling tool for

predicting performance. Using this numerical approach, a methodology for testing and predicting the performance of the Zephyr turbine will be developed.

4.2.1 Zephyr Turbine Design and Modifications

Zephyr Alternative Power, a Toronto based company was started by Ed Tsang, inventor of the Zephyr turbine, a novel vertical axis wind turbine (VAWT). Research collaboration between Zephyr and UOIT aims at developing and improving the performance of this wind generator. In a city setting, the wind is always changing direction and the velocity and is never consistent. The Zephyr VAWT is an effective machine for such conditions, so it expand the wind energy resource of a city greatly by utilizing resources that traditional horizontal axis wind turbines cannot. It is an omni-directional design, allowing the turbine to spin and produce power regardless of the wind direction.

The proprietary elements of the design are the stator blades, which help it perform better in low velocity and high turbulence wind conditions. The proprietary stator design involves an angled outer tip that creates a low pressure zone behind and draws more air into the turbine. This also helps the turbine perform well in close proximity to obstructions and other turbines. This is an advantage for elimination of wake effects, where several turbines are operating in close proximity to each other in urban areas. Figure 4.1 shows a schematic of the Zephyr turbine with its unique patented features.

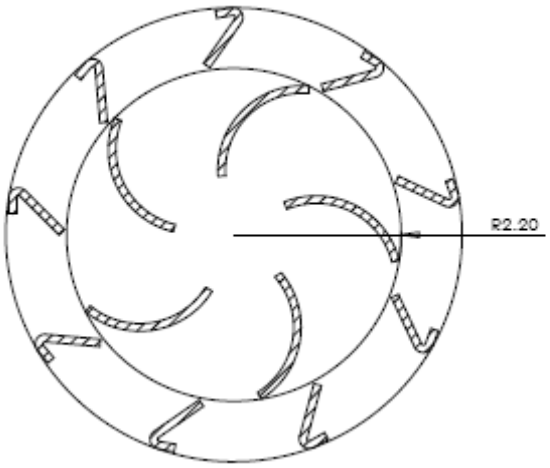

Figure 4.1a Design drawings of Zephyr VAWT

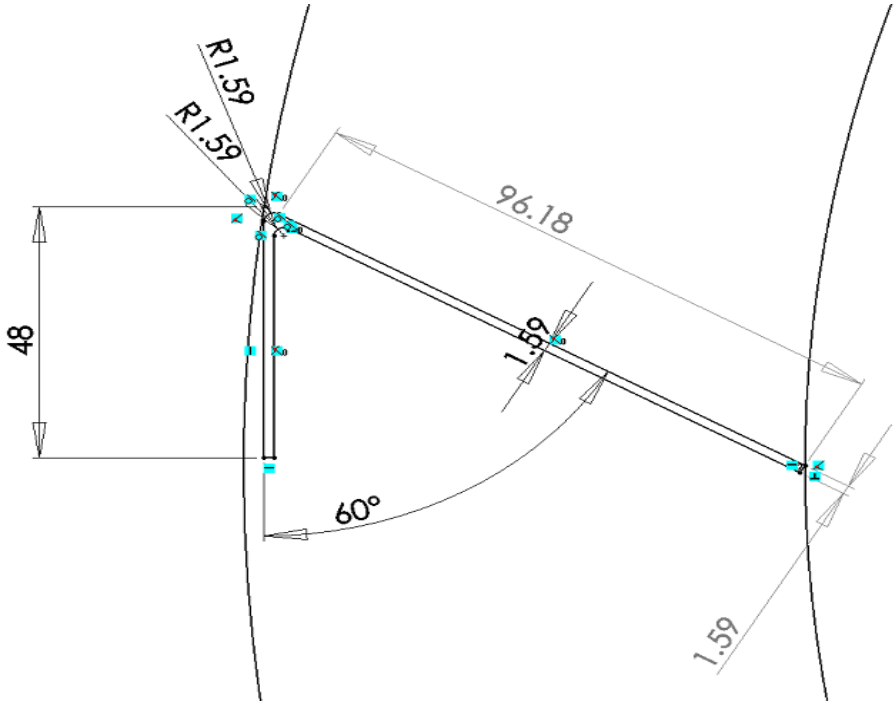

Figure 4.1b: Design drawings of Zephyr VAWT showing the outer vane stators.

The Zephyr wind turbine has several design features that can be improved upon for further increase in performance. By allowing space in the center of the rotor cage for air to flow, lift is enhanced across the blade profile, instead of the usual drag forces associated with fully closed Savonius (pure drag) rotors. Zephyr has conducted several experiments with different configurations for the top plate on the turbine. By opening or closing the top, it will be able to promote better fluid flow through the rotor. In this thesis, a detailed investigation of the effect of rotor blade geometry modification will be conducted. Fig. 4.1b shows the turbine stator-tab new dimensions set up that was used alongside the 9-blade configuration. The length of the tab, stator, and angle between them varies from the base design (see appendix E) chosen dimension by a margin of 30% in length and 15^0 in angle between. It is assumed this could create more induce low pressure vortex the will enhance more wind entrenchment into the turbine.

The blade geometry and its aerodynamic characteristics are crucial to achieve maximum energy from the wind. Like all wind turbines, only a part of the energy characterized by the Betz limit can be extracted. If too much kinetic energy were removed, the exiting air flow would become stagnant and cause blockage. In designing the optimum blade rotor, there are many tradeoffs. If a rotor with a small blade area is used, a large flow rate will be experienced through the rotor, while the pressure drop will be small. This will imply a reduction in power output. On the other hand, if a rotor with a large blade area is used, the pressure drop is large, but the flow rate will be low. The consequence is that power output will be reduced. A

good optimization and configuration of the rotor blade is therefore needed to achieve most efficient performance. A good turbine blade arrangement reduces the velocity of the flow to two-thirds (2/3) of the free stream velocity at the rotor and the minimum velocity downstream is to one-third (1/3) for better energy conversion [10].

The geometry of a turbine affects the pressure field and boundary layer along the surface. Curved blades incrementing from the traditional 2-blades Savonius VAWT have shown a high power coefficient [23]. The geometrical spacing between the Zephyr turbine rotor blades will be investigated, as well as increasing the blade number, flow and blade angle spacing. In order to keep the blade solidity constant, the dimension of the cord will be reduced as the number of blades increases. A higher blade number has the advantage of reducing blade tip losses. This is particularly evident for a vertical axis wind turbine that is noted for low rotor speed. A fast spinning rotor like the case of horizontal axis wind turbines usually has two to three blades. Fast spinning rotors have fewer blades while a slow spinning rotor should have more blades to save tip losses.

The Zephyr stator tab accelerates the air in a residential area and hence can provide more energy in the lower part of the boundary layer, where wind speed is relatively low and turbulent in a concentrated area. The other optimization of importance is the use of tabs on the ends of the stator blades to induce low-pressure

vortices in certain sections of the flow, and thereby entrain more air to enter the turbine.

4.3. Computational Procedure

A Multiple Reference Frame (MRF) will be used in the computational model for the numerical simulations. This model uses the time averaged information to predict the turbine performance. It analyzes the fluid flow with either a stationary reference frame or rotating reference frame. The model provides a convenient and effective tool to investigate the characteristic power curves for the turbine. For the Multiple Reference Frame formulation, the model is divided into two sub-domains, one for the rotor and another for the stator. The rotor sub-domain is rotating with respect to the inertial frame in the model. At the boundary between the rotor and stator sub-domains, continuity of the absolute velocity is enforced to provide appropriate values of velocity for each sub-domain [1, 10, 13]. The features of the Multiple Reference Frame solution parameters will be summarized in section 4.3.2. This model does have a limitation in accounting for high stator – rotor interaction that exists. Nevertheless, it can give valuable results for flow predictions.

4.3.1 Mathematical formulation

A Computational Fluid Dynamics algorithm defines how a discrete control volume interacts with another. The finite volume algorithm is based on a conservation principle that relates the changes in flow variables inside a control

volume to the net flux of the variable through the control volume surface. The mathematical equations are called conservation relations. The algorithms that strictly enforce these relations are called finite volume solvers. The CFD software, Fluent, is such a finite volume solver.

A typical problem might be characterized with a time-dependent separated flow at a high Reynolds number. A simplified turbulence model is considered often for the purpose of analysis. The influence of viscosity is often assumed confined to a thin layer of fluid flow adjacent to the solid surface and the vorticity is confined within the wake region, such as the sharp edges of a blade. In reality, the effect of viscosity leads to finite cores of rotational fluid. An overview of how the finite volume solver works in the computation of mathematical equations is highlighted next.

4.3.2 Governing Equations

The fundamental objective of rotor aerodynamics is to predict the induced velocity field and the performance of the rotor. Estimating the performance of the Zephyr turbine, as governed by its geometry and operating conditions, requires a CFD analysis. The velocity and pressure fields are obtained by solving the partial differential equations representing the mass and momentum conservation, using the finite volume technique. Other procedures are the finite difference method and the finite element method.

The flow field near a vertical axis wind turbine is represented by the incompressible Navier-Stokes equations. The two-dimensional governing equations for an idealized incompressible flow are derived from the basic principles of mass and momentum conservation. These principles have been applied to non-deformable, fixed control volume V, delimited by an outer surface A. The mean-flow governing equations for an incompressible fluid of density, ρ, are given as

$$\frac{\partial(\rho u)}{\partial \chi} + \frac{\partial(\rho v)}{\partial y} = 0 \tag{4.1}$$

$$\rho\left(\frac{u\partial u}{\partial x} + \frac{v\partial u}{\partial y}\right) = -\frac{\partial p}{\partial x} + \mu\left(\frac{\partial^2 u}{\partial x^2} + \frac{\partial^2 u}{\partial y^2}\right) + S_X \tag{4.2}$$

$$\rho\left(\frac{u\partial v}{\partial x} + \frac{v\partial v}{\partial y}\right) = -\frac{\partial p}{\partial y} + \mu\left(\frac{\partial^2 v}{\partial x^2} + \frac{\partial^2 v}{\partial y^2}\right) + S_y \tag{4.3}$$

where u and v are the velocities and S_x and S_y are the source terms in x and y coordinates, respectively, ρ is the density μ is the viscosity, and p is static pressure. The sources terms, S_x and S_y, are functions of the airfoil characteristics (lift and drag coefficients), the absolute velocity at the turbine blade, angle of attack, turbine radius and the angular velocity. The source terms are evaluated on part of the control volume through which the rotor blade passes. The procedure involved setting a reasonable value for the blade angle of attack in the CFD model

to compute the airfoil characteristics of the turbine blade until flow convergence was achieved.

It is necessary to specify conditions on the boundary of the domain of interest, in order to solve for the velocity field. Let x be parallel to the freestream and y be normal to the blade surface. We assume the boundary-layer thickness

$\partial x \prec\prec x$,

from which follow the same approximations as in laminar-boundary layer flow analysis:

$\bar{v} \prec\prec \bar{u}$ and $\frac{\partial}{\partial x} \prec\prec \frac{\partial}{\partial y}$

Apply in y-direction, $p = p(x)$ since $\frac{\partial p}{\partial y} \approx 0$

In Prandtl terms, 2-dimensional turbulent boundary layer approximations in horizontal flow

$$u\frac{\partial u}{\partial x} + v\frac{\partial u}{\partial y} \approx u\frac{du}{dx} + \frac{1}{\rho}\frac{\partial \tau}{\partial y}. + S_X \tag{4.4}$$

where $\tau = \begin{cases} \mu\frac{\partial u}{\partial y} - \rho uv \end{cases}$ for turbulent condition

4.3.3 Discretization of Governing Equations

The numerical solution involves discretization of the problem domain and the Navier-Stokes governing flow equations. Fluent uses the finite volume method for its discretization. The differential form of the Navier-Stokes governing equations is derived and transformed into an integral form. The solution domain is subdivided into a finite number of contiguous control volumes and conservation equations for each control volume. These equations are solved by employing FLUENT (2005) in the two-dimensional mode with no swirl. FLUENT uses a control-volume-based technique for converting the governing equations into algebraic equations that can be solved numerically. In this thesis, the solution algorithm adopted is Standard k-ε turbulence model, and a second-order upwind scheme based on a multilinear reconstruction approach is used for all dependent properties.

Reducing the integral form of the conservation equations to an equivalent algebraic expression requires spatial discretization. The finite volume method has the advantage of being applied to any type of grid, especially complex geometries. The computational nodes are located at the centroid of a control volume, as well as the boundaries.

$$\frac{\partial u}{\partial t} + \nabla \cdot \bar{F} = Q \tag{4.5}$$

$$\frac{\partial}{\partial t}\int_{\Omega} u d\Omega + \int_{S} \bar{F} \cdot d\bar{s} = \int_{\Omega} Q \cdot d\Omega \tag{4.6}$$

All finite volume solvers such as Fluent have the ability to solve the Navier-Stokes equations through an algebraic approximation. In the next section, the domain discretization for the CFD solver will be discussed.

4.3.4 Domain Discretization

A challenge in the CFD modelling was to discretize the flow domain near the blades. The solution domain is sub-divided into set of sub control volumes. A finite volume is established by all sub volumes associated with certain node after the assembly of all elements. The numerical error of the scheme changes as a function of grid spacing. Numerical error can be reduced by using a very fine grid. A practical means of indicating grid independence is comparing solutions obtained on different grids, then establishing the range of grid spacings where additional refinement does not have a significant impact on results. A combination of triangular unstructured and quadrilateral structured elements was used. Due to the importance of the fluid interaction with the blades, a more refined quadrilateral grid is used near the rotor blade edges. The grid should be fine enough to capture details of flows within these critical regions but without demanding excessive computing resources. The current method achieved a good balance between these two aspects: fine grids at blade surfaces, where accurate resolution of pressure calculations was required, and also at the surfaces of the rotor, but more coarse triangular elements for other parts of the domain (Fig. 2). More specifically, the far-field layers of elements will require less computational time than turbulent flow near the walls. The total number of elements for both grid types is illustrated in (Fig. 4.2.)

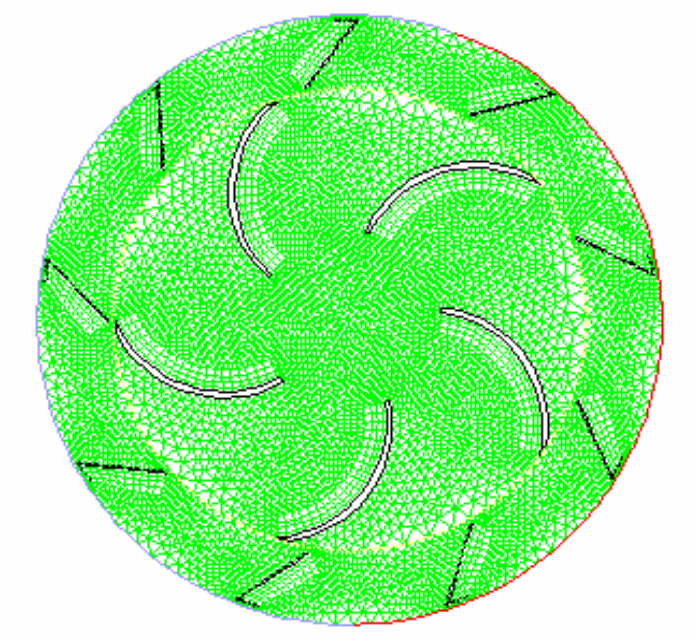

Figure 4.2a: Mesh with N = 5 and 9,202 triangular and quadrilateral elements.

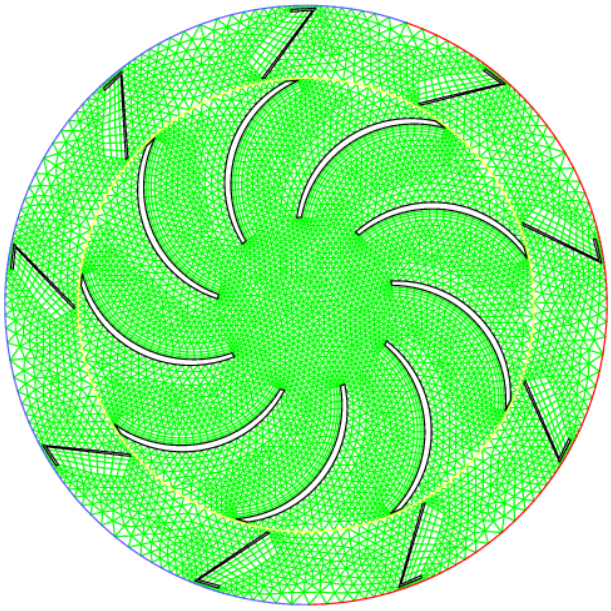

Figure 4.2b Mesh with N = 9 and 13,200 triangular and quadrilateral elements.

In mesh sensitivity studies, it is important to assess the dependence of results on grid spacing by repeating the same simulation, but with different mesh refinements. This is called a mesh sensitivity study that compares results at varying grid spacings, until the pressure coefficient on other parameters becomes nearly constant. The pressure coefficient, Kp, is defined as

$$Kp = P - P_S /(0.5\rho U_\infty{}^2) \tag{4.7}$$

where P is a measured pressure on a surface and P_s is the static pressure measured in the free stream, and U_∞ is a reference velocity taken as the free stream velocity, U. The parameter, Kp, is obtained as a CFD simulation result. The result of this grid sensitivity analysis is shown in the result section.

4.3.5 Numerical Model

The Navier-Stokes equations consist of the continuity equation, turbulence momentum equations for velocity, the energy equation and the turbulence transport equations for k and ε. These are the equations solved by FLUENT. The CFD software uses a control-volume-based technique for discretizing the fluid flow governing equations into algebraic equations that can be solved numerically

In the Multiple Reference Frame environment, FLUENT (version 6.3) uses a steady-state 2-D finite volume method with a segregated implicit solver. The Reynolds stress model constants of turbulence are used. Standard wall functions are applied for near-wall treatment and the k-ε turbulence model is used.

At the upstream boundary of the inlet, a uniform velocity with a turbulence intensity of 10% was assumed at the velocity inlet. This assumption was based on experimental data where a turbulence intensity of approximately 10% was obtained at the designated operating wind speed (Veers, Winterstein, 1997). The turbulent viscosity ratio is estimated at 1 to simulate a low turbulence viscosity (Saxena, 2007). At the pressure outlet, a backflow turbulence intensity of 12% is assumed, to account for the increased turbulence caused by interaction with the turbine. The backflow turbulence viscosity ratio was also estimated to be 1.

At the downstream boundary, the gage-pressure was assumed to be zero. On the surface of the blades and the cylinder wall, a no-slip condition was prescribed. Symmetric boundary conditions were used for both sides in the span wise direction. All stator blades were set up as stationary walls, subject to a no-slip condition with the fluid rotor modeled in the moving reference frame. The wind velocity inlet conditions are fixed at a certain mean value, as the rotor speed changes in a prescribed stepwise manner. The aerodynamic blade loads are transferred through the rotor and converted into an estimated torque on the low speed rotor shaft, resulting in energy generation from this wind turbine.

In the next chapter, 6m/s, 8 m/s, 10 m/s and 12 m/s are the selected mean wind velocities to test the design turbine rotor efficiency. A rotational speed range between 10 rad/s and 180 rad/s is used. The model is formulated with a standard second-order upwind discretization scheme using a default under-relaxation

constant. The problem is iterated until all residuals on the turbine blade walls converge to a value below the scale of 10^{-3}, at which point a valid solution is considered to be achieved. At convergence, the solution no longer changes noticeably with further iterations. All governing equations are solved in all cells to the specified convergence tolerance. Residuals were scaled relative to the local value of flow properties in order to obtain a relative error.

Convergence cannot be judged only by examining the residual levels as this could be misleading. As a secondary check for convergence, the mass and energy balances were also examined. Numerical results will be reported in the next chapter.

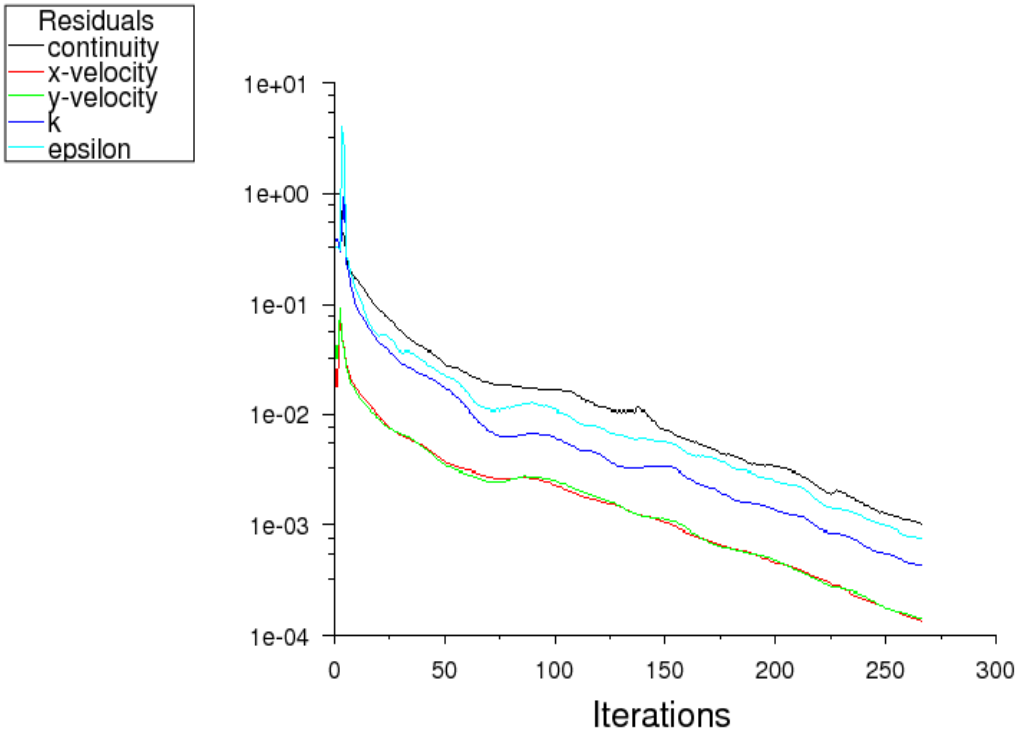

Figure 4.5: Simulation iterations convergence

Figure 4.5 shows the residual indicator when the solver has converged. It indicates that changes in flow variables typically became negligible after about 250 iterations.

4.3.6 Power Computations

Wind energy resides in the large mass of air moving over the earth's surface. This energy is available in the form of kinetic energy. Wind turbine blades receive this kinetic energy and convert it to mechanical power, then it is further converted to electrical energy. The efficiency of this conversion depends on how effectively the rotor and blades interact with the wind stream. Wind turbine technology has advanced significantly over the past few decades, and several methods of rotor/blade optimization to extract more power from the wind have been developed in the past. A force is experienced on the blades and rotor, whenever air flows across the wind turbine.

In Fluent, the rotational force and torque are computed after each time step is completed. The power extracted by the wind turbine in this CFD model is computed during post-processing. The following steps of multiplying the torque by the rotational speed are adopted:

$$P_t = \vec{T}\, x\Omega \tag{4.8}$$

$$\vec{T} = \vec{r_c}\, x\, \vec{F_P} + \vec{r_c}\, x\, \vec{F_V} \tag{4.9}$$

where $\vec{T}$ is the moment vector and $\vec{r_c}$ is the vector position originating at the centre of the rotor. Also, $\vec{F_P}$ and $\vec{F_v}$ are the pressure moment and viscous moment respectively.

A non dimensional relationship will be derived to predict the efficiency of the Zephyr VAWT for a chosen configuration. The curve of the power coefficient vs. tip speed ratio is the most important characteristic of the wind turbine, as it reflects the efficiency of a turbine in converting the wind energy into electrical energy. The power coefficient C_p is defined as

$$C_p = \frac{2 * P_t}{\rho_a V^3 2 D H} \tag{4.10}$$

This is the ratio of the shaft power extracted to the available power of the incoming airflow.

Chapter 5

RESULTS AND DISCUSSIONS

5.1 General

The key dimensionless variables for wind turbine problems are the Reynolds number, power coefficient and the tip speed ratio. The tip speed ratio and power coefficient are parameters in the thesis and they will be set within standard operating ranges. The pressure and velocity distributions will be predicted during each simulation and documented for future validation with wind tunnel testing. The data obtained from the numerical computations will be analyzed by various tools and formulae described in the previous chapters. This chapter presents simulation results in tabular form as well as graphical form and it includes a detailed analysis of the test results to explain the trends.

5.2 Performance Results

The efficiency of wind turbines is characterized by a parameter known as the coefficient of performance, or C_p. This coefficient ranges from 0 to 0.59 (see figures 3.3 and 3.5). The numerical value 0.59, or 16/27, is the Betz limit, which represents is the maximum theoretical efficiency that any wind turbine removing energy from a fluid can achieve. The C_p coefficient of a turbine is determined primarily by the aerodynamic forces, which are affected by the shape of the blades. The forces experienced by the blades will vary depending on the wind flow conditions, namely the relative velocity of the blade to the wind, or tip speed ratio.

As the tip speed ratio is varied, the rotor efficiency will change, since the blades cannot be optimized for every tip speed ratio. The curve produced by graphing the power coefficient (C_p) vs. tip speed ratio (λ) is known as the characteristic curve of the turbine. It displays the turbine's ability to operate throughout a range of conditions. The inability of VAWTs to achieve a tip speed ratio of much greater than 1 make them unable to achieve the high C_p exhibited by HAWTs, which have proven an almost 50% efficient. Typical values for VAWTs lie within the range between 0.1 and 0.18 [31]. Current developments in blade profiling and other methods are allowing vertical machines to incorporate larger lift forces, thereby increasing their performance.

Figures 5.1a and 5.1b show the starting torque vs. rotor rotational speed for different rotor blade configurations. These plots account for different mean wind velocities under varying rotor loads and speeds. The torque vs. speed plot shows agreement with the expected trends of high torque for a given VAWT rotor speed. This high torque advantage of drag-based VAWTs can be utilized for a possible hybrid of the Darrieus–Savonius turbine. The high torque becomes an advantage for a much higher efficiency, but low torque starting disadvantage for the lift-based VAWTs. The the turbine torque–speed plots are seen to be decreasing as the speed increases until the torque is nearly zero when the rotor "floats" with the wind.

Figures 5.2a and 5.2b show the corresponding power vs. rotor speed, at a given wind speed. The mechanical power converted into electrical power is a

product of the rotor torque and rotor angular speed, so it is expected from the result that the power will be zero at a zero rotor speed, and again at a high rotor speed with zero torque. The configuration with nine rotor blades has a maximum power at the lower rotor speed. The speeds at maximum power are not the same speed at which the torque is maximum in Figs. 5.1a-b. A good strategy will be to design a wind turbine that matches the rotor speed to generate maximum power as the wind velocity changes.

The power–speed and torque–speed characteristics are used to estimate the power coefficient – tip speed ratio curve of the rotor, where C_p as a function of TSR is presented. These curves are useful for predicting the turbine's ideal TSR and also its feasibility and adaptability to different wind conditions. The trends of the resultant plots follow the theoretical expected trends. The curve shapes of the power vs. function of rotor rotational velocity, and C_p vs. TSR follow a roughly parabolic shape. Figures 5.3a and 5.3b show C_p and TSR for both configurations at different wind velocities. The tip speed ratio of this turbine lies within the range between 0 and 1.2. Operating under the same condition, the N = 9 rotor blade performance appears better at a lower tip speed ratio (0.6) when compared to 0.8 for the base design with N = 5 rotor blades. The blade tip loss is minimized due to the increase of blade number and reduction of space between blades.

Figures 5.4a and 5.4b display results of the stream-tube model. The CFD and momentum model show reasonable agreement. On the left and rising branch,

there is fairly good agreement of both models, while there is some deviation in the right and falling part. The higher tip speed ratio leads to a higher value of C_p in the stream–tube model. For a low tip speed ratio where C_p values were close for both cases, the computation times are comparable. Though this validation has an error of about 20%, especially on the high TSR side, the results do follow expected trend. The CFD model with good mesh and geometry modeling yields accurate results that can be relied on compared to either the momentum or vortex models. It is also worth noting that in calculating the power using the stream tube model, we have made some assumptions in values like blade lift/drag coefficients and chord diameter. Computed average values of lift and drag coefficients obtained from CFD simulation results were substituted in the stream tube model analysis as no data for this turbine could be obtained from literature.

It is desirable to obtain a single correlation for predicting the performance of a particular turbine design at any given wind velocity. In Figs 5.3a and b, C_p and TSR at different velocities have been predicted, but it is laborious and time-consuming to perform simulations for all velocities. The coefficients were obtained at various velocities for the C_p – TSR curves for both the CFD and stream tube models. (see A .1-4 and B. 1-4) for table values. A cubic polynomial method of fitting was adopted because of its ability to give a good approximation of the curve shape with little error.

Figures 5.5a, 5.5b, 5.6a and 5.6b give the relationship between C_p and TSR for both configurations and models respectively. This relationship at all wind velocities converges to a single curve and one correlation equation. This non – dimensional relationship represents the performance of any dimensionally similar rotor, irrespective of its size, where C_p in the polynomial equation is the Zephyr wind turbine power coefficient or rotor efficiency, while x is the rotor tip speed ratio. At any given wind speed, these correlations for each configuration and model will be useful in predicting the wind turbine efficiency.

Figures 5.7a and 5.7b show each model with the different geometry modification results. The results of each model follow almost the same trend. However, the stream tube model result appears higher toward the region of decreasing rotor efficiency of the turbine. The rotor with the higher number of blades gives a higher efficiency, even at a low tip speed. An increase in the tip speed ratio that results from an incremental rotor speed favors the 5 rotor blade configuration in utilizing the energy of the wind to enhance the performance output. With fewer blades, there is a lower C_p for low tip-speed ratios. A reduction in the number of blades reduces the relative wind angle at the low design tip-speed ratio. The effect of the number of blades is negligible at the high value of design tip-speed ratio. For this reason, the Zephyr wind turbine with more rotor blades is the best choice for an area that favors a low tip speed ratio configuration. The low numbers of blades, such as three or five bladed wind turbines, use a higher tip speed ratio than the 9-blade wind turbines. This analysis will be useful when making a

decision on what configuration will give the optimum performance based on the available wind site potential.

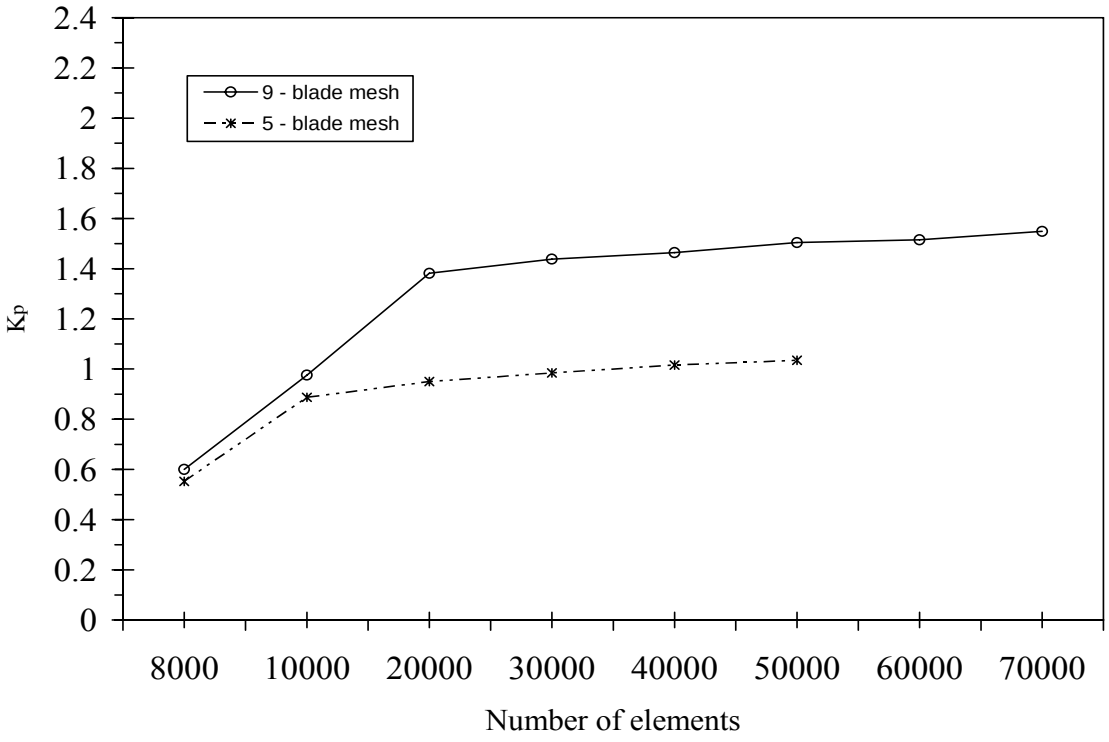

Figure 5: Predicted pressure coefficient vs. number of elements

Fig 5 shows that the pressure coefficient approaches a uniform value as the number of elements increases (mesh spacing decreases). In this case, a grid sensitivity study of the predicted pressure coefficient was the parameter. It shows that further refinement will not achieve significantly more accurate results. The plot reveals that about 15,000 and 20,000 elements for the N = 5 and N = 9 configurations domain respectively are sufficient to achieve nearly grid independent results. The choice of a higher number of elements (mesh enrichment or adaption) for domain discretization may result in little additional accuracy but there is a penalty in the extra computational effort required.

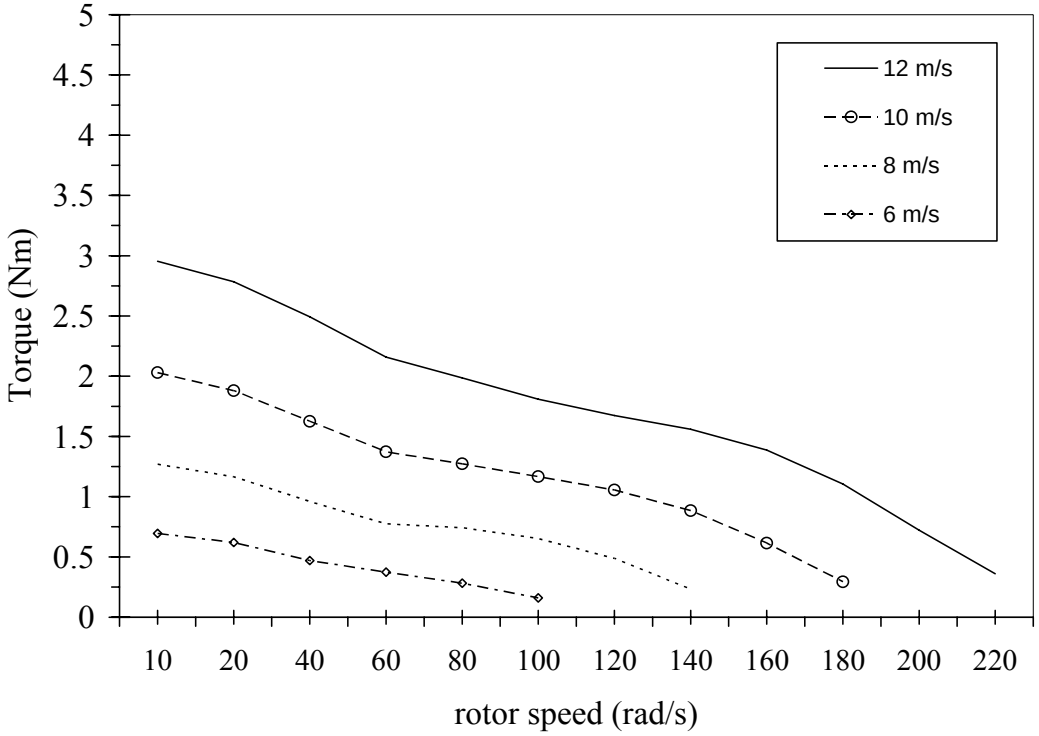

Figure 5.1a: Torque – rotor speed curves at various wind speeds for N = 5

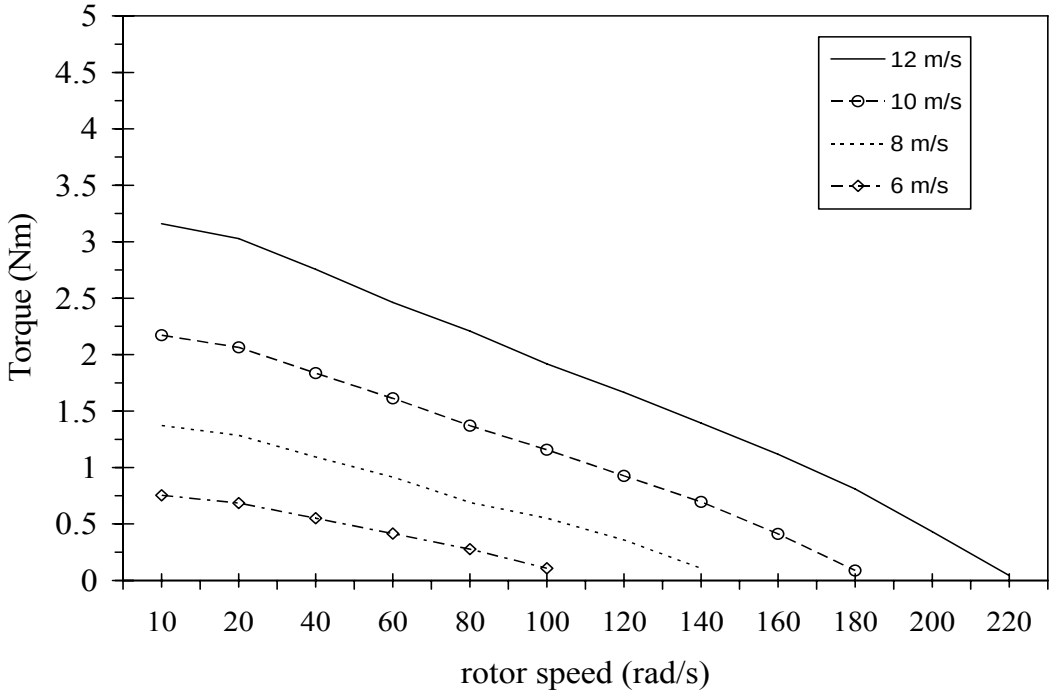

Figure 5.1b: Torque – rotor speed curves at various wind speeds for N = 9

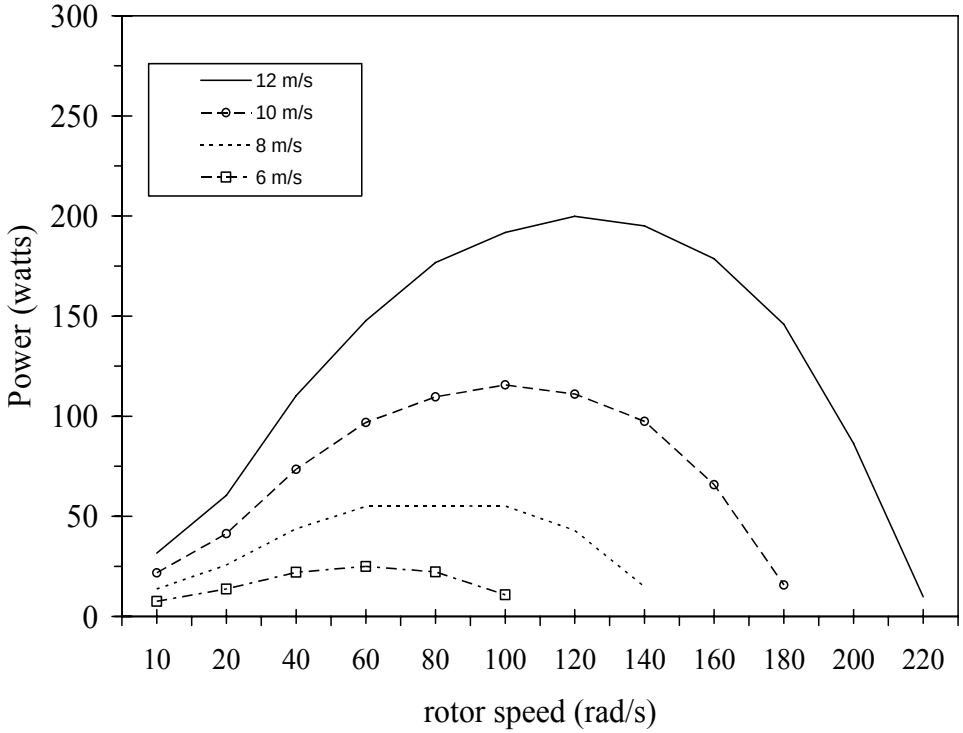

Figure 5.2a: Power–rotor speed curves at various wind speeds for N = 9

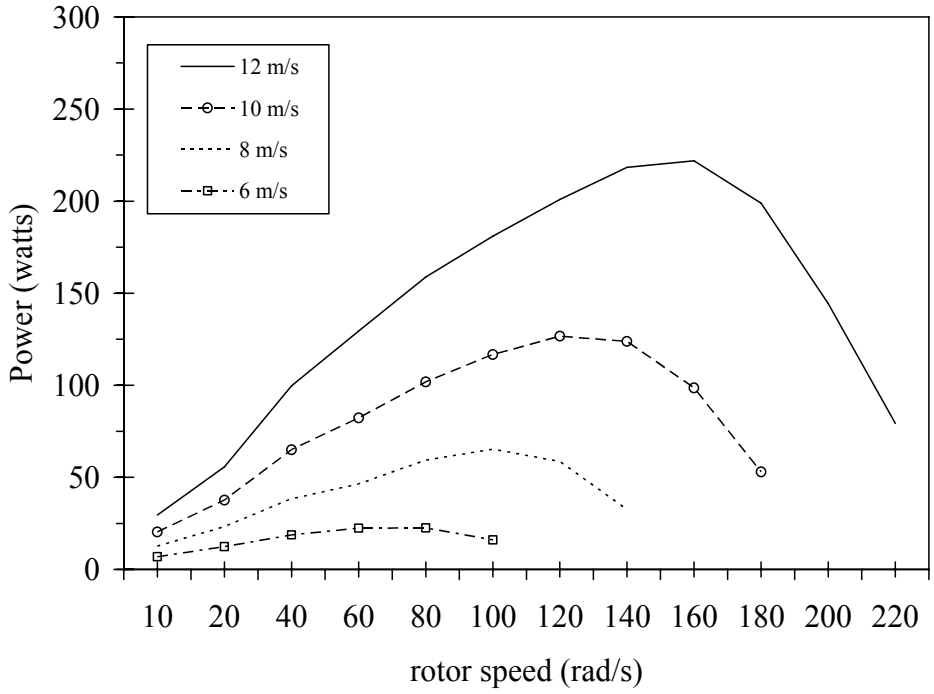

Figure 5.2b: Power–rotor speed curves at various wind speeds for N = 5.

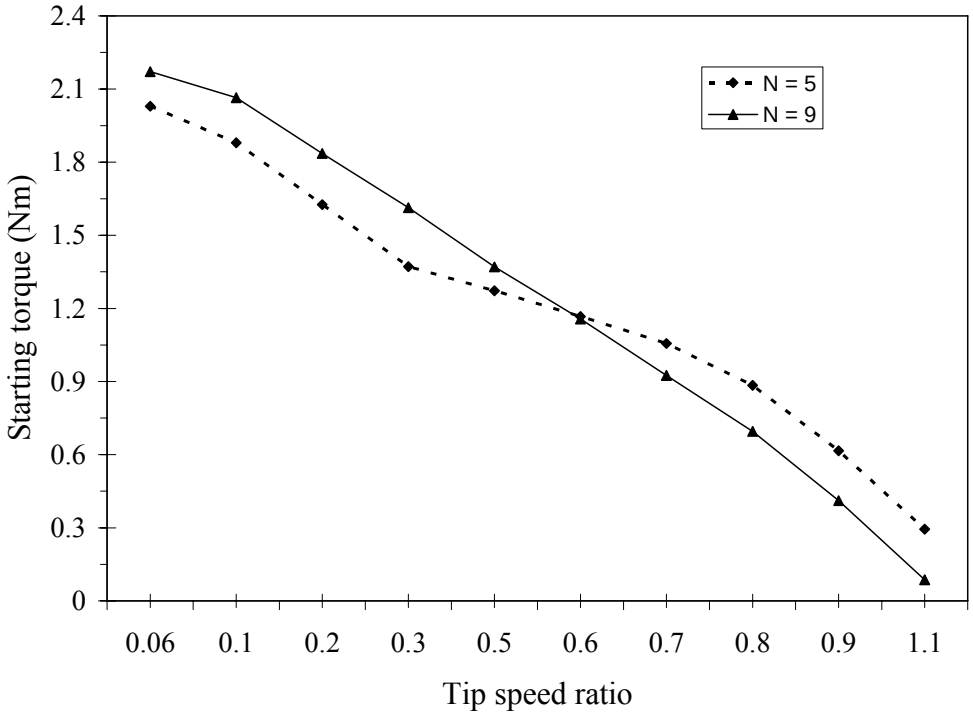

Figure 5.2c: Starting Torque vs. Tip speed ratio for N configurations

Figure 5.2c, shows results that agree with the principle of a wind turbine that starting torque is inversely proportional to the design tip speed ratio under load. As TSR increases, the load starting torque produced by the blade decreases.

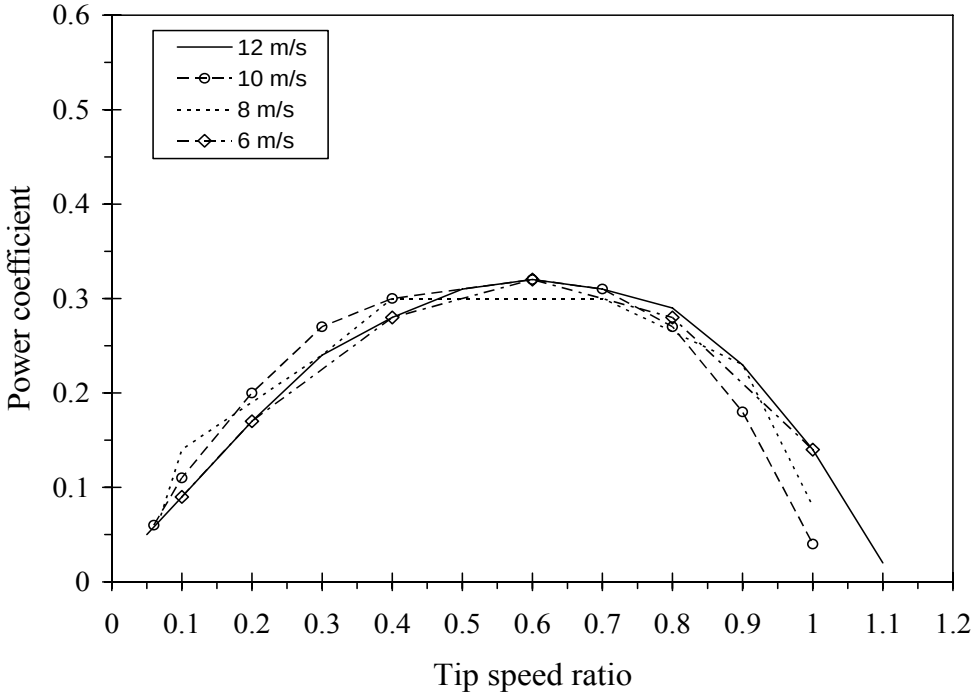

Figure 5.3a: CFD performance curves for N = 9 at various wind speeds

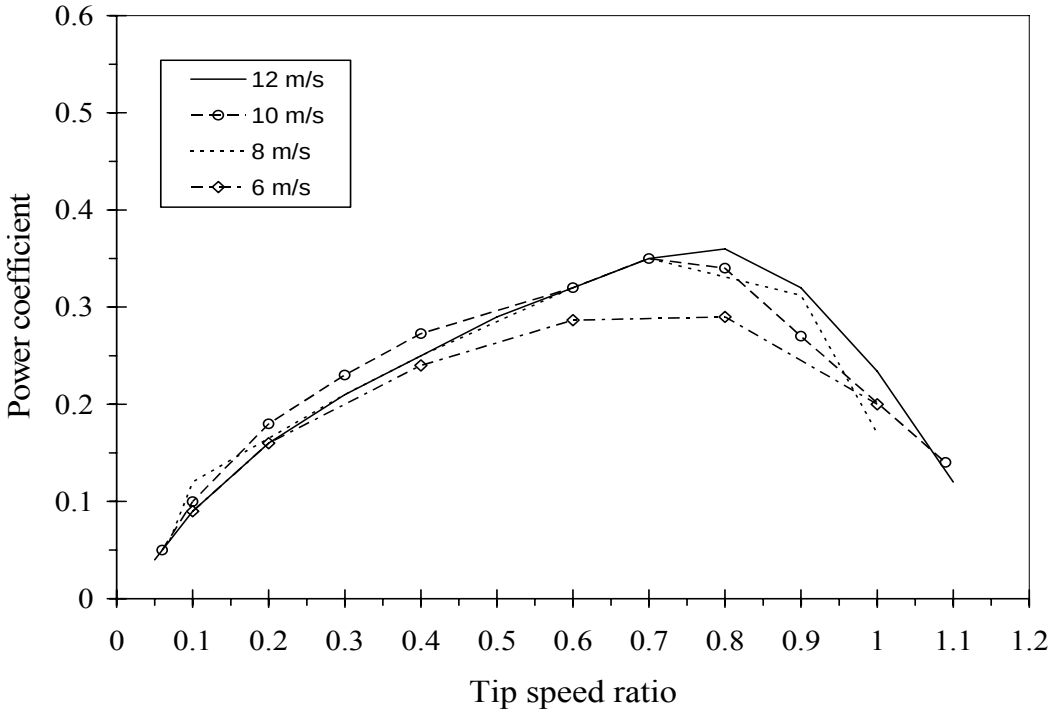

Figure 5.3b: CFD performance curves for N = 5 at various wind speeds

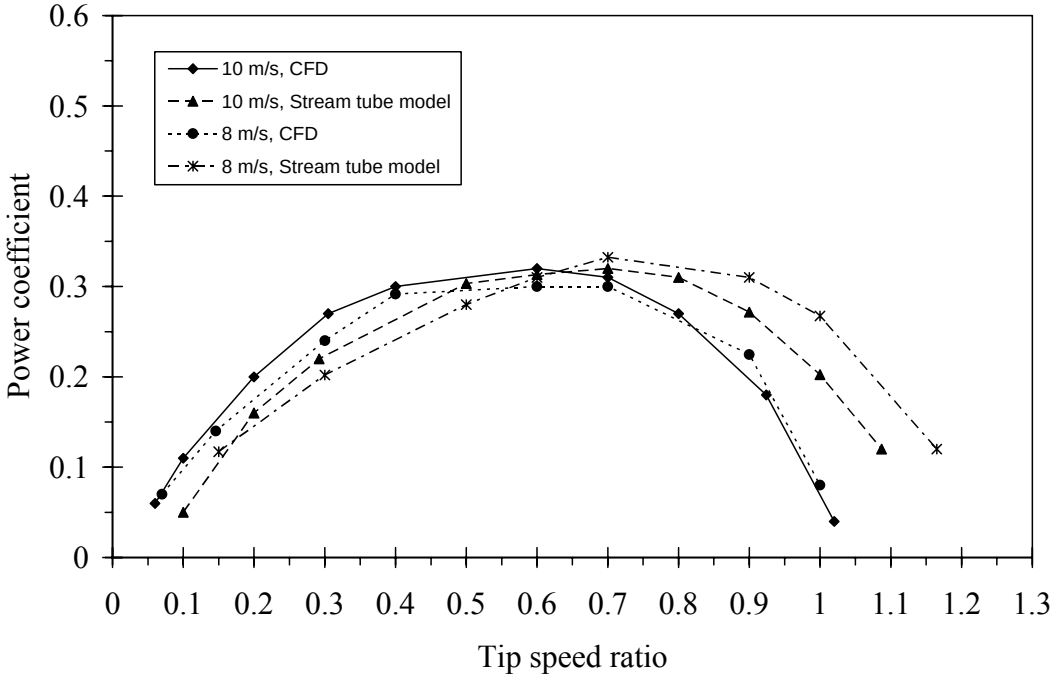

Figure 5.4a: Performance curve for both models, N = 9 at given wind speeds

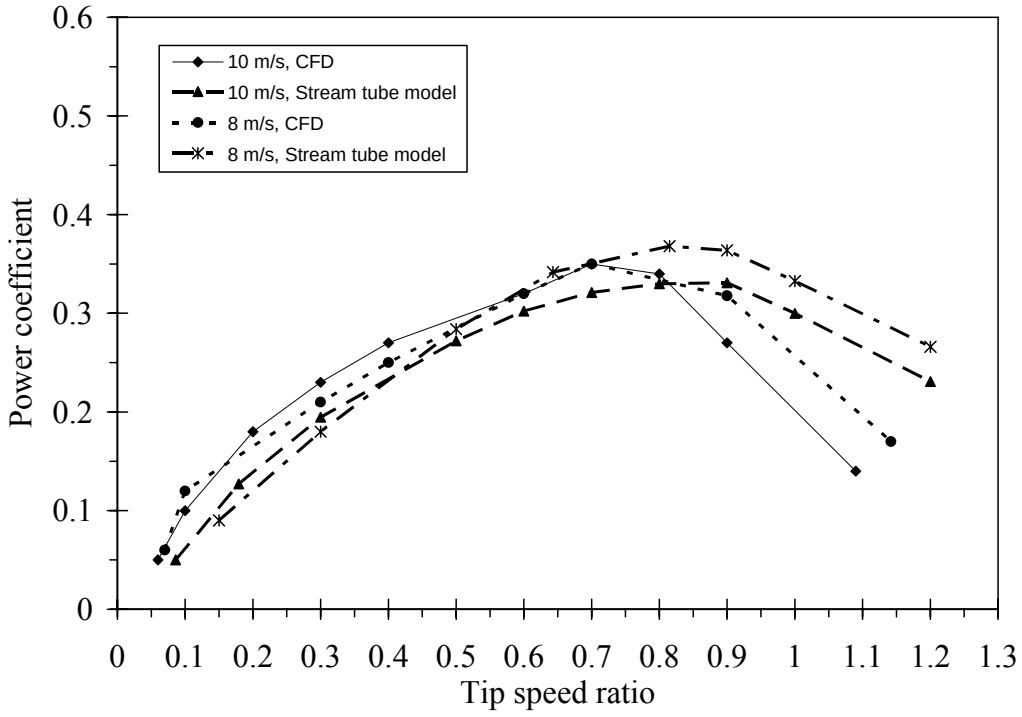

Figure 5.4b: Performance curve for both models, N = 5 at given wind speeds

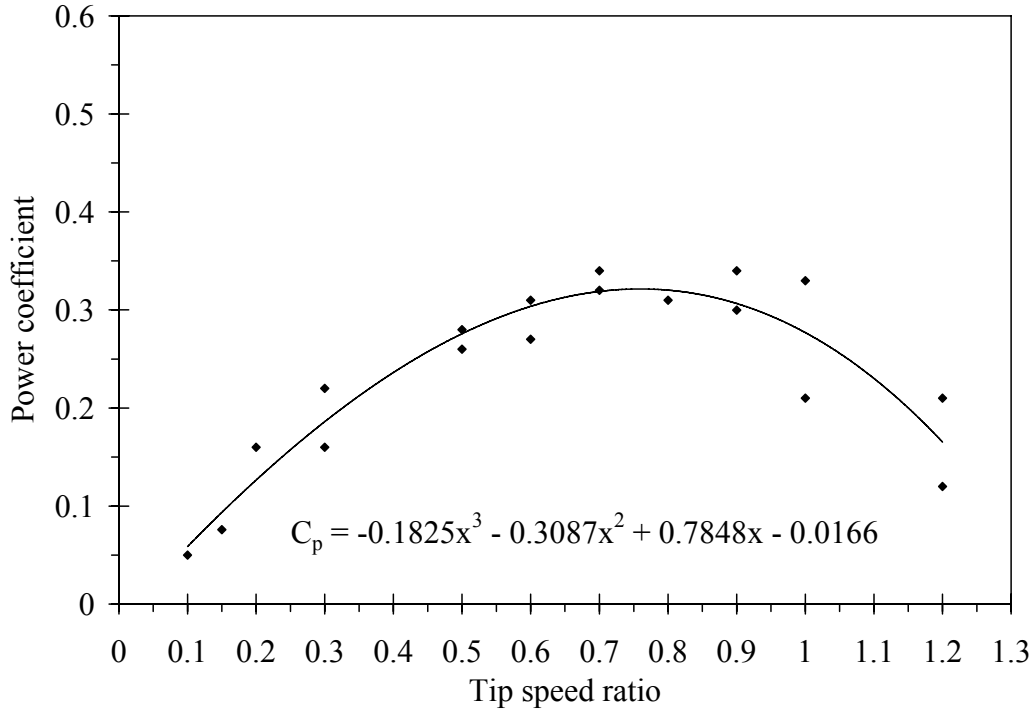

Figure 5.5a: Stream tube model prediction curve at all wind velocities for N = 9

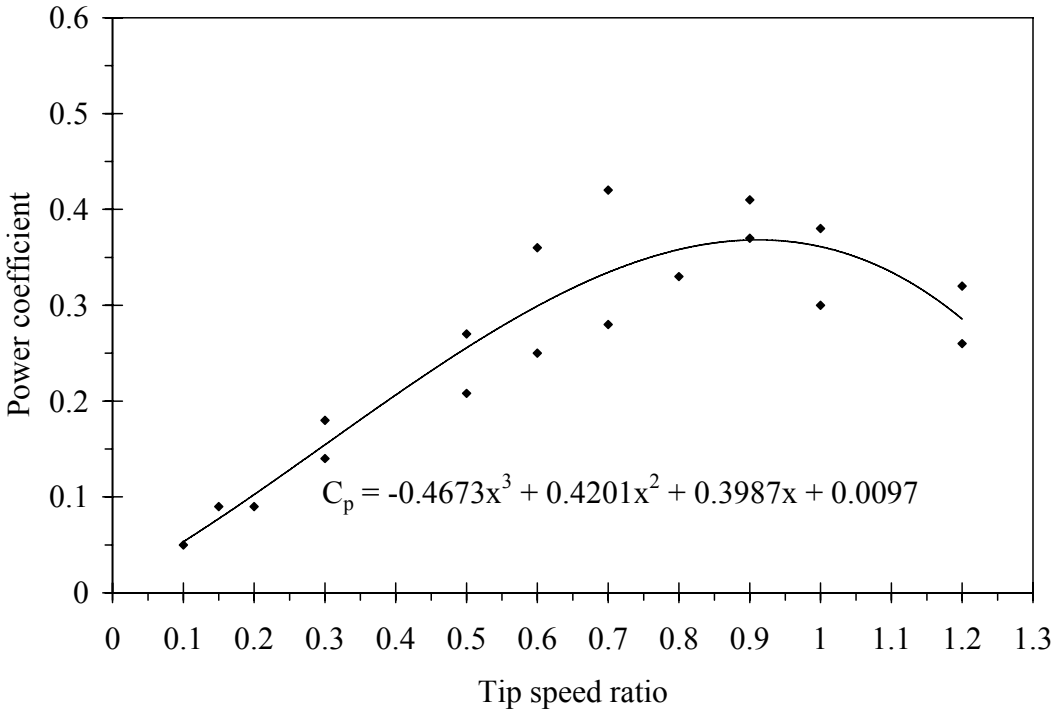

Figure 5.5b: Stream tube model predictions curve at all wind velocities for N = 5

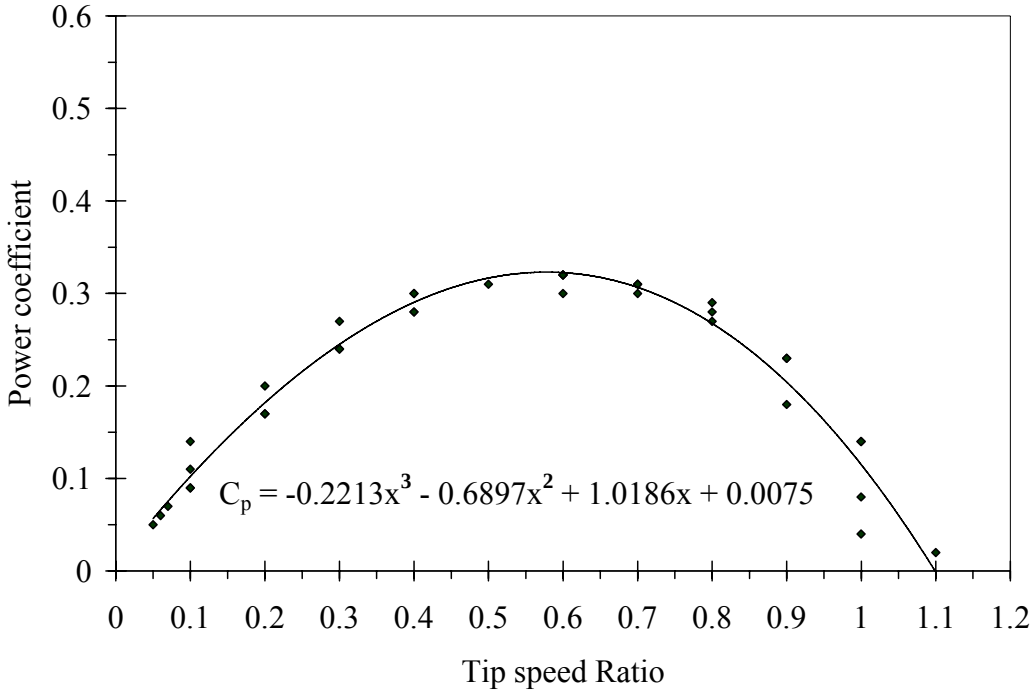

Figure 5.6 a: CFD performance prediction curve at all wind velocities for N = 9

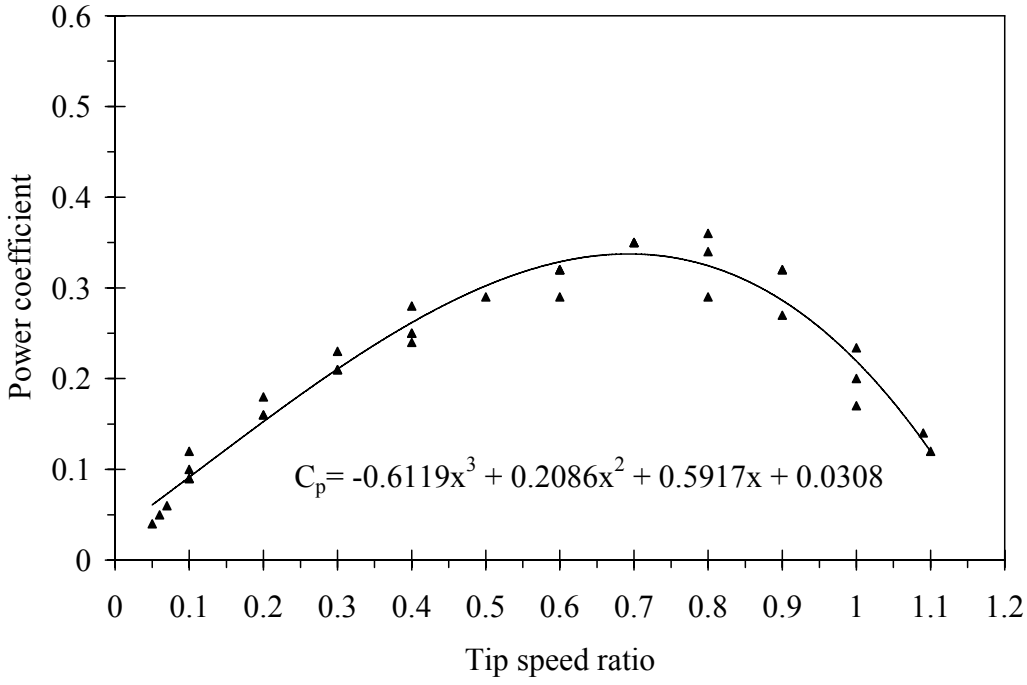

Figure 5.6 b: CFD performance prediction curve at all wind velocities for N = 5

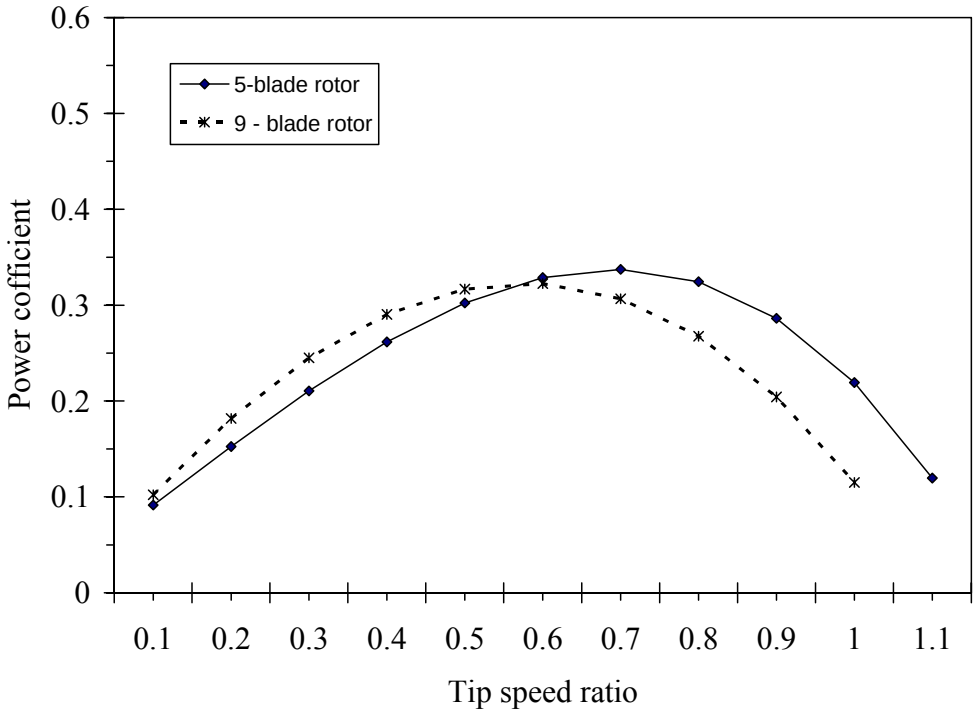

Figure 5.7 a: CFD model comparisons for N configurations

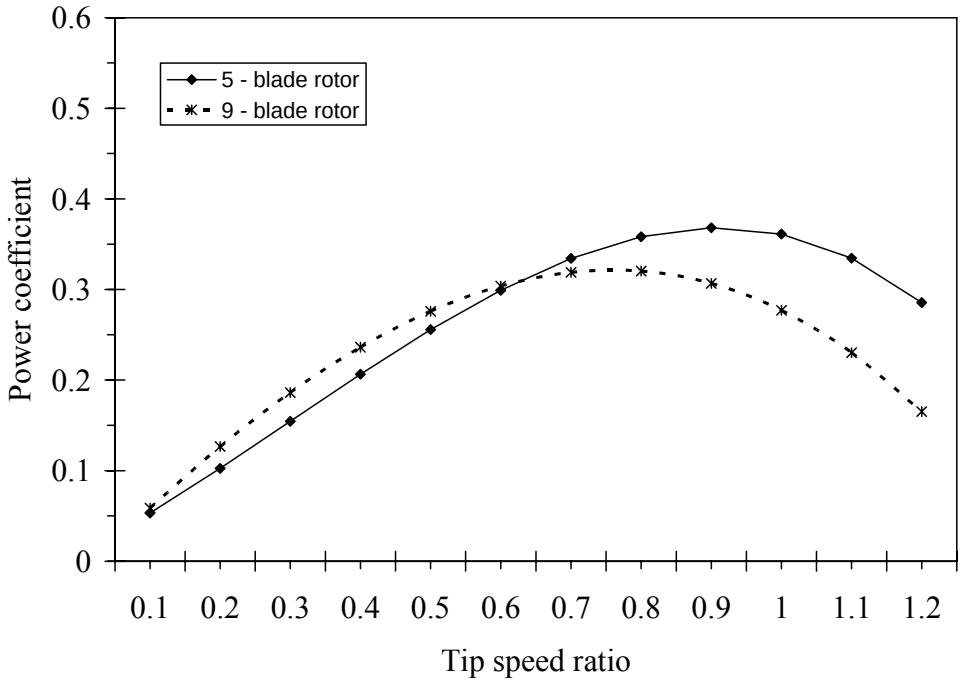

Figure 5.7 b: Stream-tube model results for N configurations

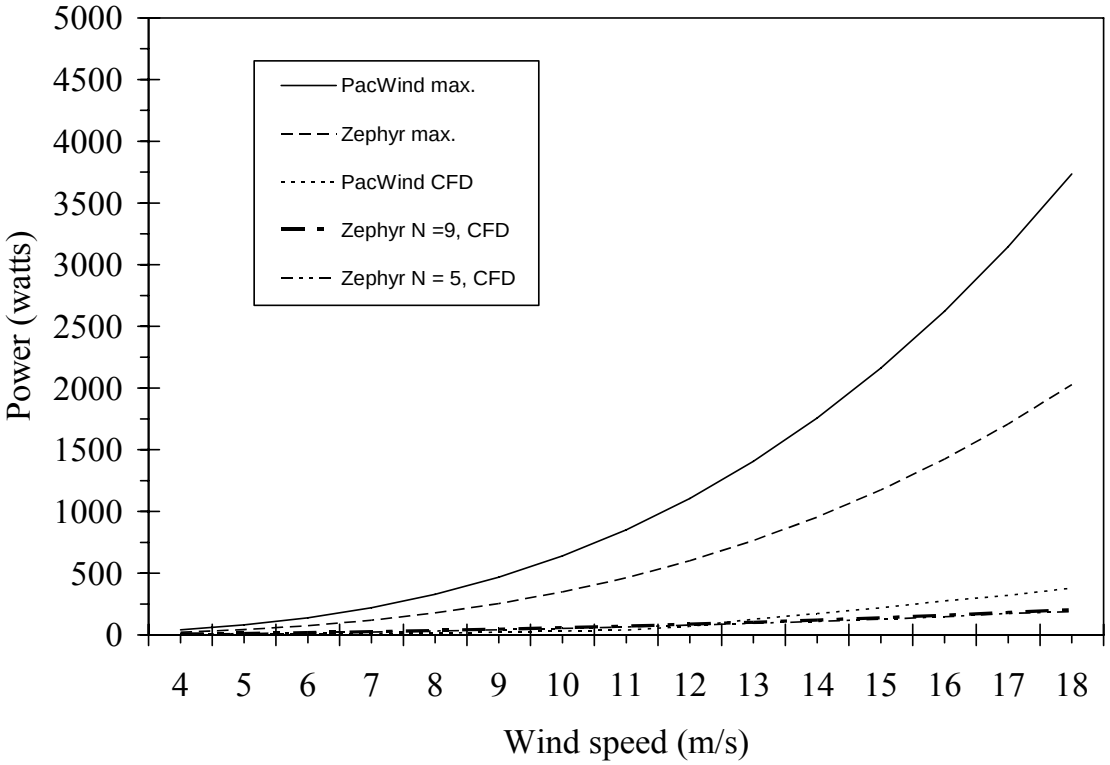

Figure 5.8a: Maximum power curves of PacWind and Zephyr turbines

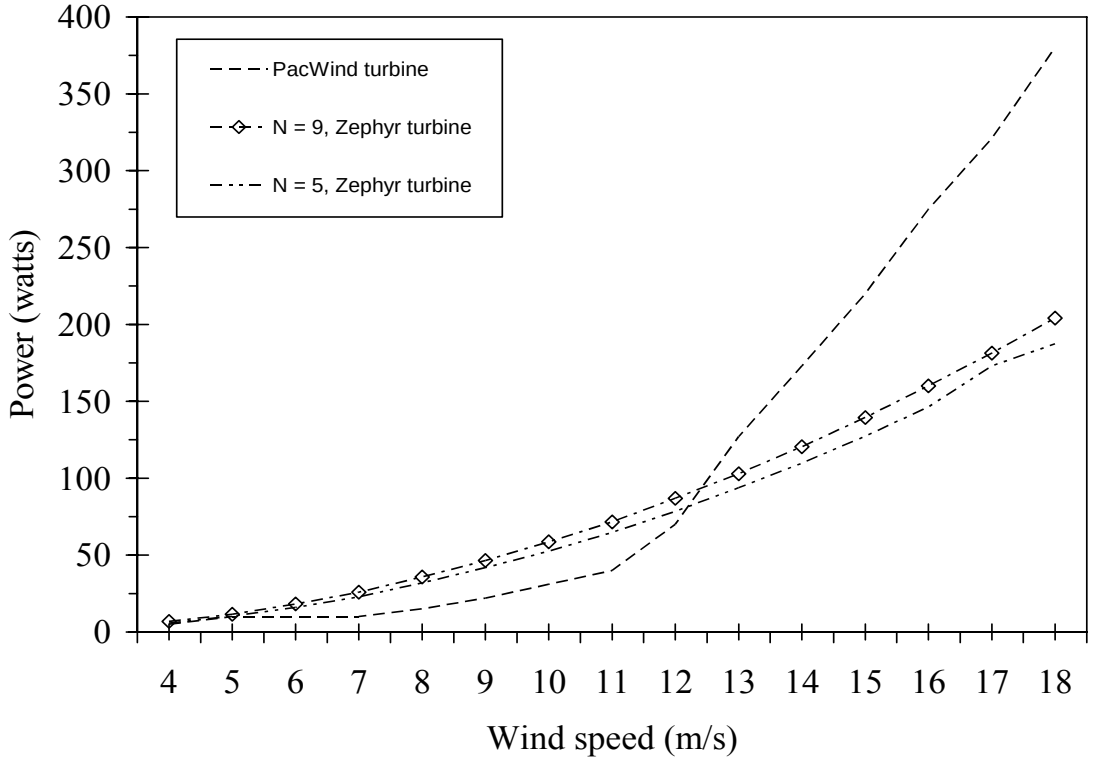

Figure 5.8b: Power vs. wind velocity for the configurations.

Results of power as a function of wind velocity are shown in Figs 5.8a and 5.8b. This plot follows reasonably close to an expected cubic shape, as power increases with the third power of wind velocity, i.e.,

$$P = \frac{1}{2}.\rho.A.V^3, \tag{5.1}$$

where ρ is the density of the air stream flowing through the turbine, A is the effective area of the rotor blades, and V is the velocity of the air flow stream. In figure 5.8a, the maximum theoretical power that can be obtained from both turbines are displayed. The PacWind maximum power curve extracts more power under the same condition of wind velocity. However, its rotor swept area is greater than the Zephyr rotor. The interest in the Pacwind turbine in this thesis is using it to compare with the Zephyr design, regarding the utility of the stator–tab, which Pacwind lacks in its configuration. Figure 5.8b indicates the unique Zephyr design has a beneficial impact.

The 9-blade configuration gives an improved rotor power output when compare the base 5-blade rotor design under the same operating conditions. It exhibits an increase of about 20% percent in power output over the five rotor blade configuration. Moreover, since the power coefficient is directly proportional to the lift forces acting on the blade, the geometry modification of the blade flow angle, blade spacing and chord diameter on the 9-blade turbine causes the lift forces acting on the modified rotor to increase. Figures 2.4 and 2.5 showed the schematic of the Zephyr vertical axis wind turbine and the Pacwind vertical axis wind turbine respectively. They very much look and operate under the same principle. The

Zephyr VAWT is uniquely different by the addition of the stator vein and tab. Given the information available from Pacwind Technology, the same conditions were imposed as the Zephyr wind generator design. A careful observation of the plot of figure 5.8 shows that during low wind speed conditions, the Pacwind turbine is unable to generate appreciable power until about 12 m/s wind velocity. The Pacwind turbine will work better in a region with high wind potential (see Appendix C for table).

The Zephyr simulation results under the same conditions exhibit a better design. Its ability to generate power under the same low wind velocity makes the Zephyr design a better and improved design for harvesting the wind energy continuously at all wind speeds. The proprietary stator blade elements of this design help it perform in low velocity wind conditions drawing more air into the turbine. It is important to observe from figure 5.8 of the difference in rotor power generated among these two designs, especially between the wind velocities 13 m/s and 18 m/s. The power from the Pacwind turbine appears higher because of its area of 55 inches by 30 inches, as compared to the Zephyr turbine of 30 inches by 30 inches for a given equal blade surface area of contact with flowing air during operation, the rotor torque and power conversion from the Zephyr turbine design will increase in Fig. 5.8.

The power output of a wind turbine is directly related to the swept area of the blades. Swept area refers to the area through which the rotor blades spin. Given

that the swept areas of both models are not equal, comparisons are inconsistent. However, a reasonable comparison can be made in terms of power generation per unit area as indicated in Figure 5.9. The results clearly show that the Zephyr turbine operates with higher power conversion efficiency at both high and low wind speed conditions.

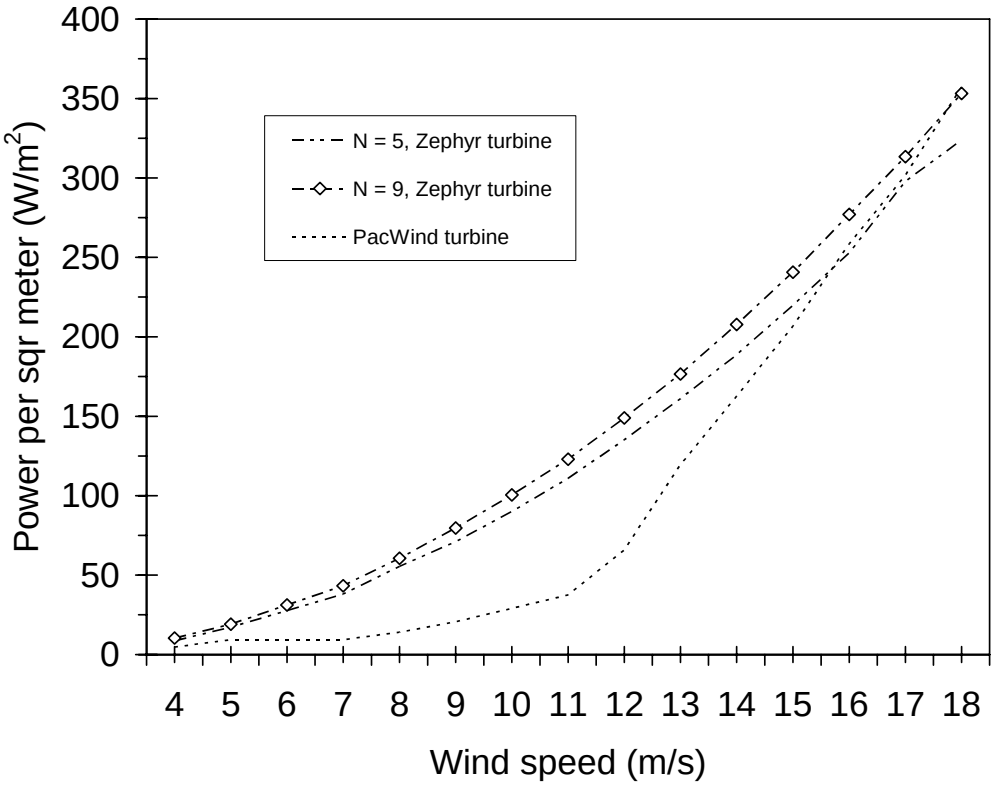

Figure 5.9: Power per square meter – wind speed curves

Drag and lift coefficient results are plotted against changing wind velocity in figures 5.10 and 5.11. As expected, the drag coefficient decreases as the wind velocity increases. The 5 rotor blade configuration has more drag force during low

velocity conditions. In figure 5.11, the lift coefficient for the 9 rotor blade configuration appears higher. An improvement in lift coefficient will result in a high lift force also. The lift force is a factor in improving the drag based turbine for electricity generation. This high value of lift coefficient for this configuration explains why the power generated for N = 9 is more than the N = 5 configuration in figure 5.8.

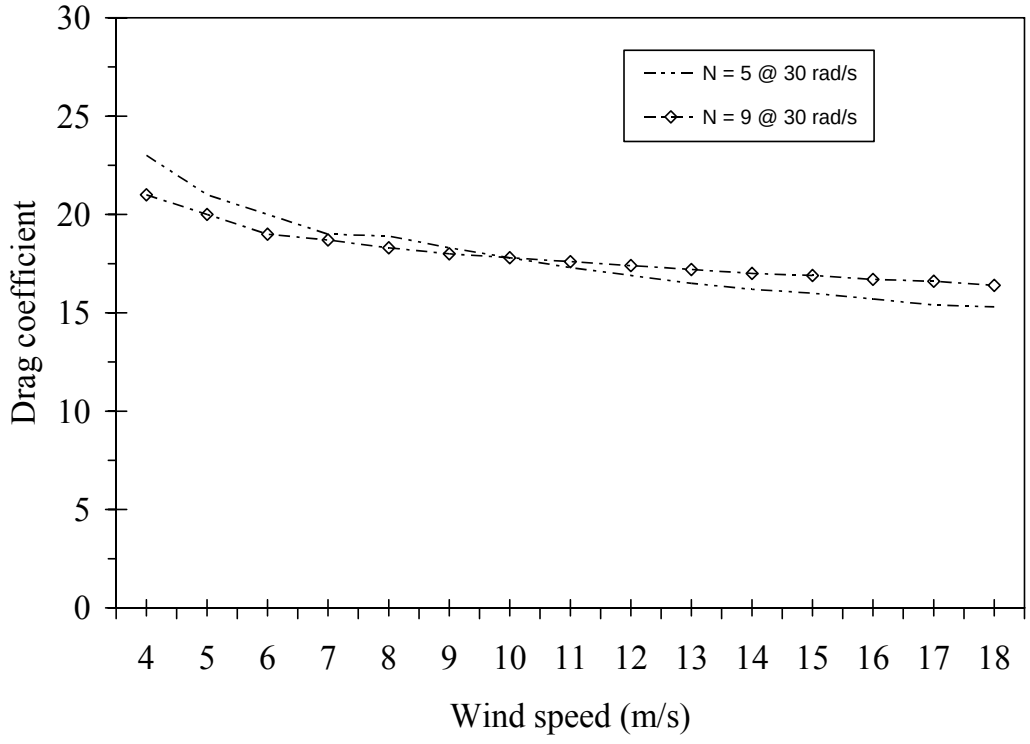

Figure 5.10: Drag coefficient vs. wind speed at different N configurations

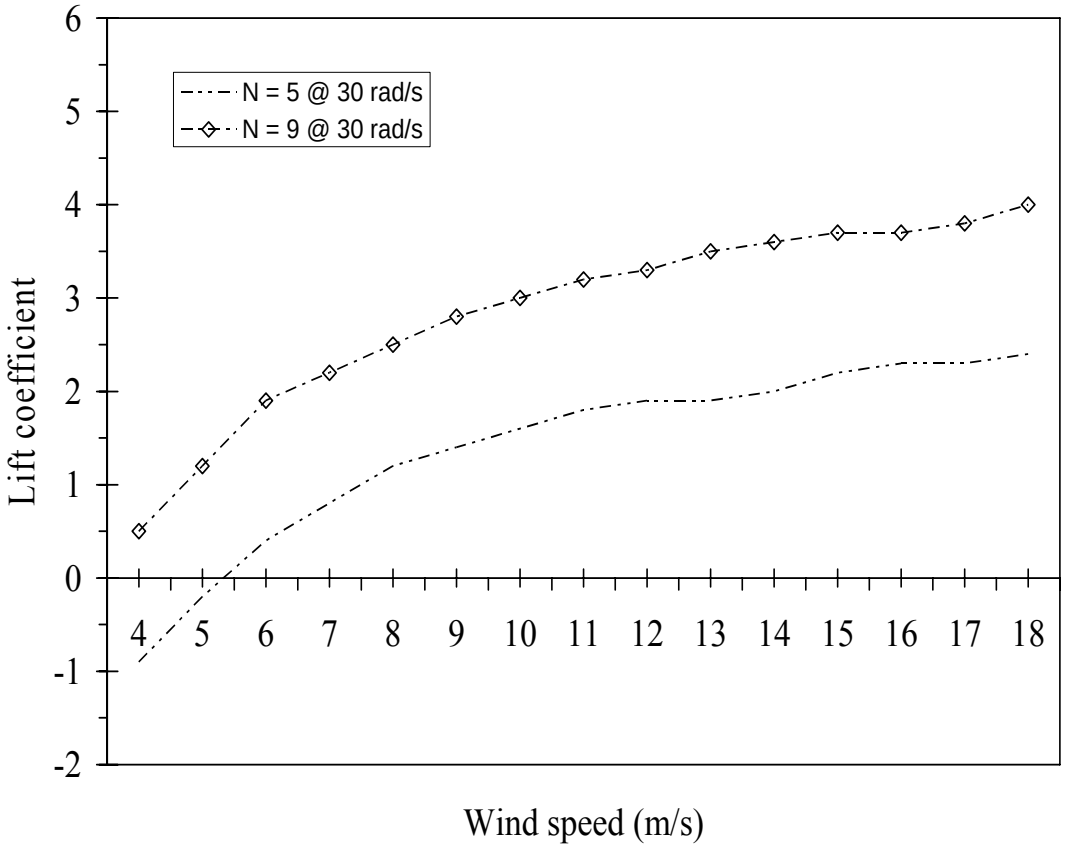

Figure 5.11: Lift Coefficient vs. Wind speed

Figures 5.12 and 5.13 show the vector profile plots of the overall flow field. The inlet velocity on the horizontal direction. On the flow inlet face, higher velocities are seen at the tip of the stator tabs and in the rotor domain. A recirculation zone with lower speeds between the stator and angle tabs arises due to the restriction caused by the stator tab length. It can be seen that the incoming airflow is blocked by the tabs and rotor. This contact between the rotor blade and the kinetic energy of the wind is crucial to harvesting power from the wind movement across the turbine. A circular accelerating zone exists behind the tabs

and rotor, which results in a low pressure near the wall of the stators. At the exit side of the stators, there also exists a near-zero velocity zone. The proprietary stator-tab elements are beneficial in low velocity and high turbulence wind conditions, as the low pressure zone entrains more air into the turbine, thereby enhancing performance.

According to the simulation results, the stators and angle tabs of the Zephyr vertical axis wind turbine does improves its power performance by accelerating the airflow through the rotor. The modification made to the base design of 5-blade rotor configuration in term of the stator tab length and angle increment as well as in rotor blades increased to 9, resulted in power output boost. Figure 5.12 gives an indication of an increased air flow velocity from the stator tab inlet.

Figures 5.14 and 5.15 show the contours of static pressure distribution in the turbine. This reflects the total energy distribution both on the inner rotor and outer stators. The contour profile shows a significant increase in pressure as the wind comes in contact with the stators and at the other inlet region with low velocity, the pressure then decreases as it flows into the rotor sub-domain, except where it is directly funneled at the blade. The wind energy entering from the inlet side is blocked by the wind turbine rotor blades, which capture some of the energy. The pressure indicated in figs 5.14 and 5.15 are in terms of gauge pressure. The pressure terms can be converted to absolute pressure using atmospheric pressure (about 101 kPa).

The negative pressures predicted at the centre and exit part of the turbine blades are advantageous to the Zephyr VAWT. This is as a result of improved efficiency of the turbine, which requires increased contribution from the lift force to generate additional torque.

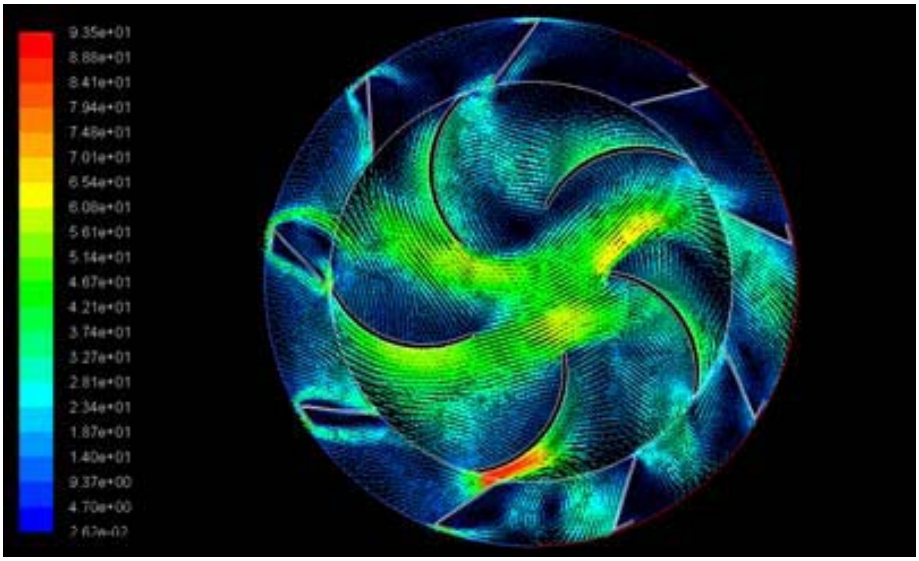

Figure 5.12: Predicted velocity vectors (m/s) for N = 5

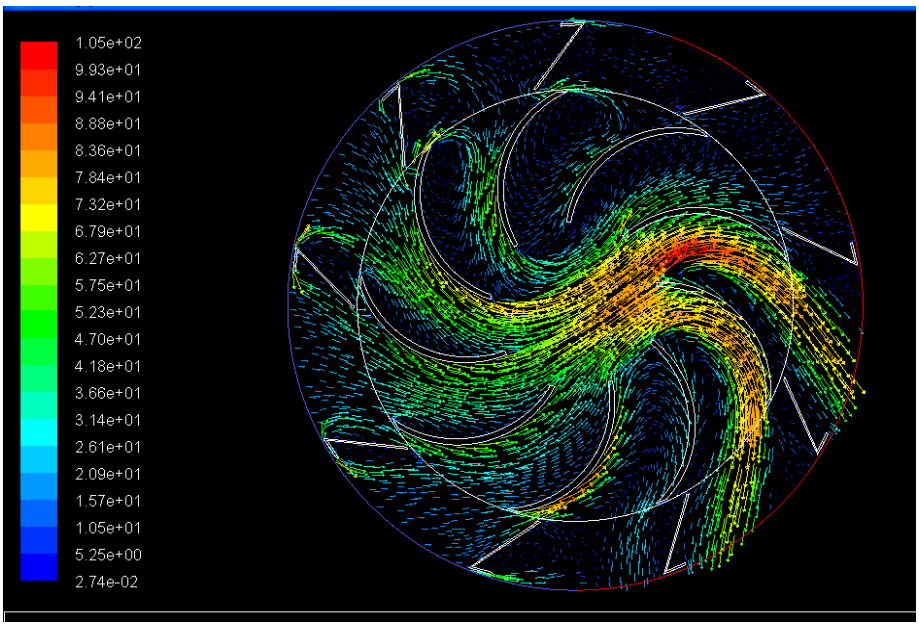

Figure 5.13: Predicted velocity vectors (m/s) for N = 9

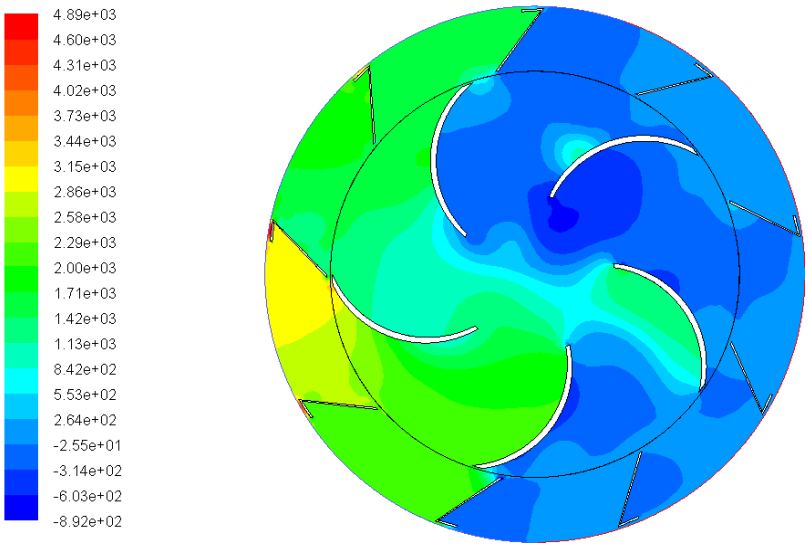

Figure 5.14: Contours of static pressure (kPa) for N = 5

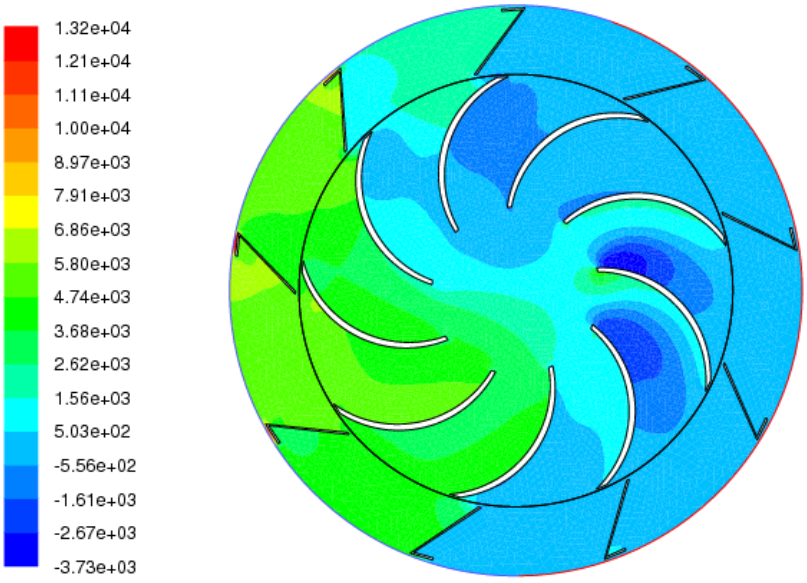

Figure 5.15: Contours of static pressure (kPa) for N = 9

Chapter 6

CONCLUSIONS AND RECOMMENDATIONS

Applications

The omni-directional ability of the Zephyr VAWT to extract wind energy from any direction is advantageous over a conventional HAWT of the same capacity. The added benefit of continuous power generation, regardless of low or high wind velocity, places this particular design ahead of others in the VAWT category. Furthermore, its aesthetic appearance, which many consider attractive, can make it acceptable to be installed on top of a building, as an added architectural feature.

The Zephyr vertical axis wind turbine has wide application ranges from urban areas and cities where fluctuation in wind speed are not problematic, to rural areas and open farms where turbulence does not pose a limitation to its operation.

Figure 6.1 – Zephyr VAWT in a city. www.zephyrpower.com/prod.html

6.1 Summary and Conclusions

CFD has been a useful modeling tool for analyzing the performance of a Zephyr wind turbine. It is an inexpensive and effective method of simulating and testing a large number of models that could not be readily examined in a wind tunnel. Small design changes can be studied with these models, and tested quickly. In this thesis, a 2-D numerical analysis has been completed using a multiple rotating reference frame formulation, to predict time averaged results. A grid independence study verifies the solution independence on grid spacing. From the performance curves, an optimum tip speed ratio was acquired. This performance characteristic was determined based on a modified rotor blade configuration. The results are useful in determining the optimal number of rotor blades depending on different wind speeds. The stator of the proprietary Zephyr design enhanced the performance, especially in low wind speed zones. Also, a stream tube momentum model was used in a theoretical analysis to predict the VAWT performance. The results showed close agreement with computed values from the CFD model. A single non-dimensional polynomial correlation for different blade for configurations was obtained. These relationships can be used to predict and represent the performance of any dimensionally similar turbine rotor, irrespective of size. These correlations can also be used to predict the performance without CFD simulations.

From the above studies, the newly developed Zephyr vertical axis wind turbine was found to be unique and more efficient in harvesting wind energy. It has an excellent self-starting ability due to its high torque value. Even at low wind

velocity, it does still run smoothly, high torque and high rotor speed which make it a good choice for electricity generation in cities and rural area. The Zephyr VAWT is a technology that favours wide applications due to its ability to be installed on any location irrespective of prevailing changing wind speed. The rotor speed (RPM) can be improve upon through further geometry optimization of the turbine by enhancing it lift force contribution. The stator tab variation for optimum geometry search does proved advantage in performance.

6.2 Recommendations

This energy conversion device is highly efficient in its ability to operate under low or high wind operating condition. We encourage its commercialization especially in cities. Its scalable size favors installation on building roof top to. I strongly believe further optimizing the stator-tab of this unique VAWT will boost its power output. Future research in this subject is very important; recommendations listed below are focused on enhancing the performance features, modeling methods and other validation work for the Zephyr VAWT.

6.2.1 CFD modeling

Further research should investigate the model using a sliding mesh formulation, as this will allow for more detailed investigation into the rotor-stator interaction. The multiple reference frame capability of Fluent is unable to account for this effect. The sliding mesh formulation requires a high capacity computer for

modeling and simulation. A complete 3-D CFD simulation should be performed. This offers the possibility of visualizing the fluid flow phenomena and more detailed quantitative data of the flow through the turbine. Unlike the 2-D model, the 3-D modeling and simulation will help to investigate the end effects of the turbine. Optimization of the stator tab geometry would also become possible. Given the small margin of power output from the N = 9 rotor blade configuration over the N = 5 configuration, I recommend the optimization of the stator/tab should be done on the N = 5 rotor blades if material and construction cost is a determining factor.

6.2.2 Wind tunnel testing

There is little or no available experimental data for this type of Zephyr VAWT. Wind tunnel testing of this turbine will give more actual data to validate the CFD simulation. Experimental testing in a controlled condition will give results that measure the turbine non-dimensional performance curve without, freestream variations. Such experiments would provide more useful data on the effectiveness of the proprietary design elements and allow recommendations to be made about further areas of improvement for the Zephyr VAWT. These results will then be compared with the CFD modeling simulations to verify the predictions.

REFERENCES

[1] Ackermann, T., So der, L., "An Overview of Wind Energy – Status 2002" *Renewable and Sustainable Energy Reviews*, vol. 6, pp. 67 – 128, (2002)

[2] "Wind Energy costs", part of the National Wind Coordinating Committee's *Wind Energy Series*, No. 11, 01 (1997)

[3] American Wind Energy Association, "Global Wind Energy Market Report", http://www.awea.org/pubs/documents/globalmarket2003.pdf March 7, 2002

[4] Dorn, J.G., Earth Policy Institute, "Wind Indicator Data", http://www.earth-policy.org/Indicators/Wind/2008.htm March 4, 2008

[5] Global Wind Energy Council, "Global Wind 2006 report", http://www.gwec.net/index.php?id=78 June 2006

[6] Wind Hydrogen Limited. http://www.wind-hydrogen.com/concept_wind%20hydrogen.html Sept. 5, 2006

[7] Golding, E. W., "The Generation of Electricity by Wind Power", London E. & F. M. Spon Ltd, Halsted Press, 1976

[8] Canadian Wind Energy Association, "Wind Energy-Powering Canadian Future", http://www.canwea.ca/production.stats.cfm. Accessed Nov.22, 2006

[9] Sim˜ao, C. J., Ferreira, G., Bussel, G .V and Kuik, G. V. "Wind tunnel hotwire measurements, flow visualization and thrust measurement of a VAWT in skew." *44th AIAA Aerospace Sciences Meeting and Exhibit/ASME Wind Energy Symposium*, 2006.

[10] Spera, D. A., “Wind Turbine Technology”, ASME Press, 1998

[11] Manwell, J. F., McGowan, J. G., Rogers, A. L., “Wind Energy Explained; Theory, Design and Application”, John Wiley & Sons Ltd, 2002, Amherst.

[12] Kovarik, T., Pipher, C., Hurst, J., “Wind Energy”, Prism Press, 1979

[13] Akiyoshi Iida, Akisato Mizuno, Keiko Fukudome, Numerical Simulation of Aerodynamic Noise Radiated form Vertical Axis Wind Turbines, *Proceedings of the 18 International Congress on Acoustics*, 2004, CD-ROM

[14] Ammara, I., Leclerc, L., and Masson, C., “A Viscous Three Dimensional Differential/ Actuator-Disk Method for the Aerodynamic Analysis of Wind Farms,” *Journal of Solar Energy Engineering*, vol. 124, pp. 345 - 356, November, 2002.

[15] Abe, K., Nishida, M., Sakuraia, A., Ohya, Y., Kiharaa, H., Wadad, E., Satod, K., 2005. “Experimental and numerical investigations of flow fields behind a small wind turbine with a flanged diffuser.” *Journal of Wind Engineering and Industrial Aerodynamics.* Vol. 93, pp. 951–970.

[16] Wang, F., Bai, L., Fletcher, J., Whiteford, J., Cullen, D., “The methodology for aerodynamic study on a small domestic wind turbine with scoop.” *Journal of Wind Engineering and Industrial Aerodynamics,* vol. 96, pp. 1-24, (2008).

[17] Sim ao Ferreira, C.J., Bijl, H., Bussel, G.V., Kuik, G.V., “Simulating Dynamic Stall in a 2D VAWT: Modeling strategy, verification and validation with Particle Image Velocimetry data” The Science of Making Torque from Wind. *Journal of Physics*: Conference Series 75, pp. 012023, (2007)

[18] Kume, H., Ohya, Y., Karasudani, T., Watanabe, K., "Design of a shrouded wind turbine with brimmed diffuser using CFD." *Proceedings of the Annual Conference of JSAS*, pp. 51–54, (2003)

[19] Sorensen, J.N., Kock, C.W. "A model for unsteady rotor aerodynamics using CFD". Journal of Wind Engineering and Industrial Aerodynamics, vol. 92, pp. 315–330. (2004)

[20] Templin, R.J., "Aerodynamics Performance Theory for the NRC Vertical-Axis Wind Turbine," N.A.E. Report LTR-LA-160, June 1974

[21] Hahm, T., Kroning, J. "In the Wake of a Wind Turbine," Fluent News, vol. 11, no. 1, pp. 5-7, spring 2002.

[22] Kelecy, F., "Wind Turbine Blade Aerodynamics," Fluent news, vol. 11, no.1, pp. 7, spring 2002.

[23] Newman, B.G., "Measurements on Savonius Rotor with Variable Gap," *Proceedings of the sherbrooke University Symposium on Wind Energy*, Sherbrooke, Canada, 1974, p. 116.

[24] Camporeale S M, Fortunato B, and Marilli G, "Automatic System for Wind Turbine Testing," *Journal of Solar Energy Engineering*, vol. 123, pp. 333-338, 2001.

[25] The Energy Blog
http://thefraserdomain.typepad.com/energy/2008/05/worlds-largest.html
May 15, 2008

[26] Patel, M.R. (1999) Wind and Solar Power Systems, CRC Press, NY.

[27] Paul Cooper and Oliver Kennedy "Development and Analysis of a Novel Vertical Axis Wind Turbine" University of Wollongong, Wollongong, 3 (2005)

[28] Fluent 6.2 Users Guide (2005). The MRF Formulation. Modeling Flows in Moving and Deforming Zones, no. 10.3.2.

[29] Saxena, Amit (2007). Guidelines for the Specification of Turbulence at Inflow Boundaries. Retrieved October 30, 2007 from http://support.esi-cfd.com/esi-users/turb_parameters/

[30] Veers, P.S., & Winterstein, S.R. (1997). Application of Measured Loads to Wind Turbine Fatigue and Reliability Analysis. ASME Wind Energy Symposium.

[31] Gasch, R. Twele, J. (2002). Wind Power Plants, Fundamentals, Designs, Construction and Operation. Solarpraxis AG.

[32] Aerodynamics Physics Organization. http://hyperphysics.phy-astr.gsu.edu/Hbase/pber.html April, 2001

[33] Paraschivoiu, I., Double-Multiple Streamtube Model for Studying Vertical-Axis Wind Turbines, AIAA Journal of Propulsion and Power, Vol. 4, pp. 370-378. 1988.

[34] Naterer, G.F., and Pope, K., Effects of Rotor–Stator Geometry on Vertical Axis Wind Turbine Performance, Technical Report, University of Ontario Institute of Technology, Oshawa, Ontario, 2007

[35] Thirty-Year Average of Monthly Solar Radiation, 1961-1990. "*Renewable Resource Data Center"*. http://rredc.nrel.gov/solar/old_data/nsrdb/redbook/sum2/state.html. Accessed April 28, 2007

APPENDIX

Appendix A 1-4: Computed Torque, C_p and TSR (λ) values, N = 9 Rotor blades configuration.

U = 12 m/s

N (rpm)	Torque (N-m)	Power (Watts)	λ	C_p
10	3.1597	31.5976	0.0503	0.0513
20	3.0276	60.5536	0.1007	0.0984
40	2.7556	110.2258	0.2014	0.1792
60	2.4625	147.7518	0.3021	0.2402
80	2.2087	176.7027	0.4028	0.2873
100	1.9182	191.8208	0.5035	0.3119
120	1.6654	199.8573	0.6042	0.325
140	1.3934	195.0821	0.7049	0.3172
160	1.1165	178.6534	0.8056	0.2905
180	0.8102	145.8468	0.9063	0.2371
200	0.4318	86.36	1.007	0.1404
220	0.0444	9.779	1.1077	0.0159

A.2: Computed Torque, C_p and TSR (λ) values, N = 9 Rotor blades configuration.

U = 10 m/s

N (rpm)	Torque (N-m)	Power (Watts)	λ	C_p
10	2.171	21.717	0.0604	0.061
20	2.064	41.285	0.1208	0.116
40	1.835	73.416	0.2416	0.206
60	1.613	96.789	0.3625	0.271
80	1.37	109.626	0.4833	0.308
100	1.156	115.646	0.6042	0.3249
120	0.925	111.008	0.725	0.3119
140	0.695	97.398	0.8458	0.2736
160	0.411	65.796	0.9667	0.1848
180	0.086	15.636	1.0875	0.0439

A.3: Computed Torque, C_p and TSR (λ) values, N = 9 Rotor blades configuration.

U = 8 m/s

N (rpm)	Torque (N-m)	Power (Watts)	λ	C_p
10	1.371	13.716	0.075	0.0752
20	1.284	25.694	0.151	0.141
40	1.093	43.759	0.302	0.2401
60	0.915	54.924	0.453	0.3014
80	0.69	55.209	0.604	0.303
100	0.551	55.118	0.755	0.3025
120	0.357	42.915	0.906	0.235
140	0.105	14.792	1.057	0.081

A.4: Computed Torque, C_p and TSR (λ) values, N = 9 Rotor blades configuration.

U = 6 m/s

N (rpm)	Torque (N-m)	Power (Watts)	λ	C_p
10	0.754	7.5438	0.1007	0.0981
20	0.685	13.716	0.2014	0.1784
40	0.551	22.047	0.4028	0.2868
60	0.415	24.932	0.6042	0.3243
80	0.277	22.209	0.8056	0.2889
100	0.107	10.769	1.007	0.1401

Appendix B.1: Computed Torque, C_p and TSR (λ) values, N = 5 Rotor blades configuration.

U =12 m/s

N (rpm)	Torque (N-m)	Power (watts)	λ	Cp
10	2.954	29.54	0.05	0.048
20	2.783	55.676	0.1	0.094
40	2.494	99.771	0.201	0.1622
60	2.159	129.54	0.302	0.2106
80	1.986	158.902	0.403	0.2584
100	1.81	181	0.504	0.2943
120	1.673	200.863	0.605	0.3266
140	1.559	218.338	0.706	0.355
160	1.386	221.894	0.807	0.3608
180	1.104	198.88	0.905	0.323
200	0.721	144.27	1.009	0.2346
220	0.36	79.349	1.11	0.129

Appendix B.2: Computed Torque, C_p and TSR (λ) values, N = 5 Rotor blades configuration.

U = 10 m/s

N (rpm)	Torque (N-m)	Power (watts)	λ	C_p
10	2.029	20.294	0.06	0.057
20	1.879	37.591	0.121	0.105
40	1.625	65.024	0.242	0.1827
60	1.371	82.296	0.363	0.231
80	1.272	101.803	0.484	0.286
100	1.167	116.713	0.605	0.327
120	1.055	126.674	0.726	0.355
140	0.884	123.855	0.848	0.348
160	0.615	98.552	0.969	0.279
180	0.294	52.943	1.09	0.148

Appendix B.3: Computed Torque, C_p and TSR (λ) values, N = 5 Rotor blades configuration

U = 8 m/s

N (rpm)	Torque (N-m)	Power (watts)	TSR	C_p
10	1.27	12.7	0.075	0.069
20	1.165	23.317	0.151	0.127
40	0.96	38.404	0.302	0.21
60	0.774	46.482	0.454	0.255
80	0.742	59.375	0.605	0.325
100	0.652	65.278	0.757	0.358
120	0.488	58.582	0.908	0.321
140	0.231	32.466	1.06	0.178

Appendix B.4: Computed Torque, C_p and TSR (λ) values, N = 5 Rotor blades configuration.

U = 6 m/s

N (rpm)	Torque (N-m)	Power (watts)	TSR	C_p
10	0.695	6.959	0.1009	0.09
20	0.619	12.395	0.201	0.161
40	0.469	18.79	0.403	0.244
60	0.373	22.402	0.605	0.291
80	0.281	22.555	0.807	0.293
100	0.16	16.002	1.009	0.208

Appendix C – Power curve

Rotor speed of 30rpm

Wind velocity. (m/s)	Zephyr N=5, Power (W)	Zephyr N=9, Power (W)	Zephyr Max Power (W)	PacWind Power (W)	PacWind Max Power (W)
4	5	6	22	5	40
5	10	11	43	10	80
6	16	18	75	10	138
7	22	25	119	10	219
8	32	35	178	15	327
9	41	46	253	22	466
10	52	58	347	31	640
11	64	71	462	40	852
12	78	86	600	70	1106
13	93	102	763	127	1407
14	109	120	954	173	1757
15	127	139	1173	220	2161
16	146	160	1424	275	2623
17	172	181	1708	321	3146
18	187	204	2027	380	3735

Appendix C-2, Power/square swept area curves

Wind velocity. (m/s)	Zephyr N=5, Power (W/m^2)	Zephyr N=9, Power (W/m^2)	PacWind Power (W/m^2)
4	8.65	10.38	4.69
5	17.31	19.04	9.39
6	27.7	31.16	9.39
7	38.08	43.28	9.39
8	55.4	60.59	14.09
9	70.98	79.63	20.67
10	90.02	100.41	29.13
11	110.8	122.92	37.59
12	135.04	148.89	65.78
13	161.01	176.59	119.36
14	188.71	207.75	162.59
15	219.87	240.65	206.76
16	252.77	277	258.45
17	297.78	313.36	301.69
18	323.75	353.185	357.14

Appendix D: Design drawings of Zephyr turbine

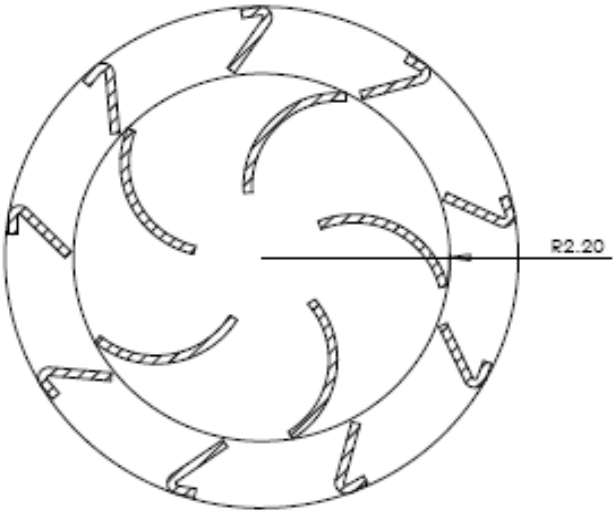

SECTION A-A

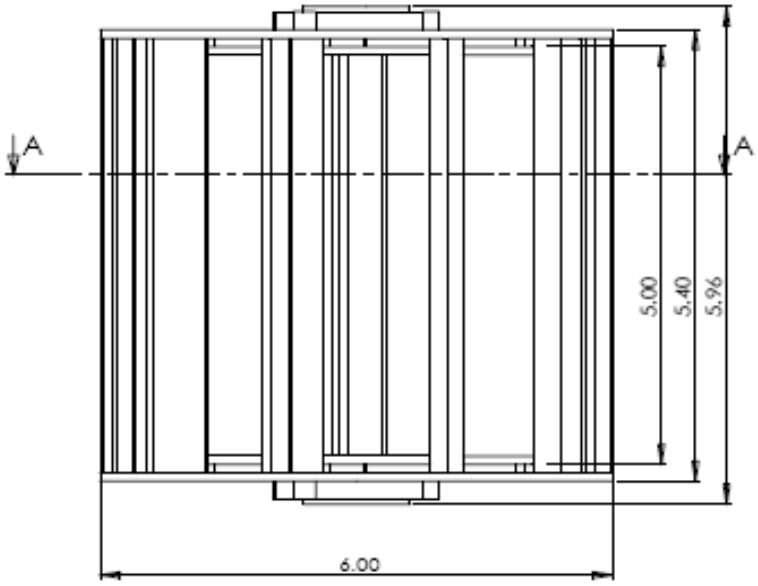

Appendix E: Stator – tab base design dimensions

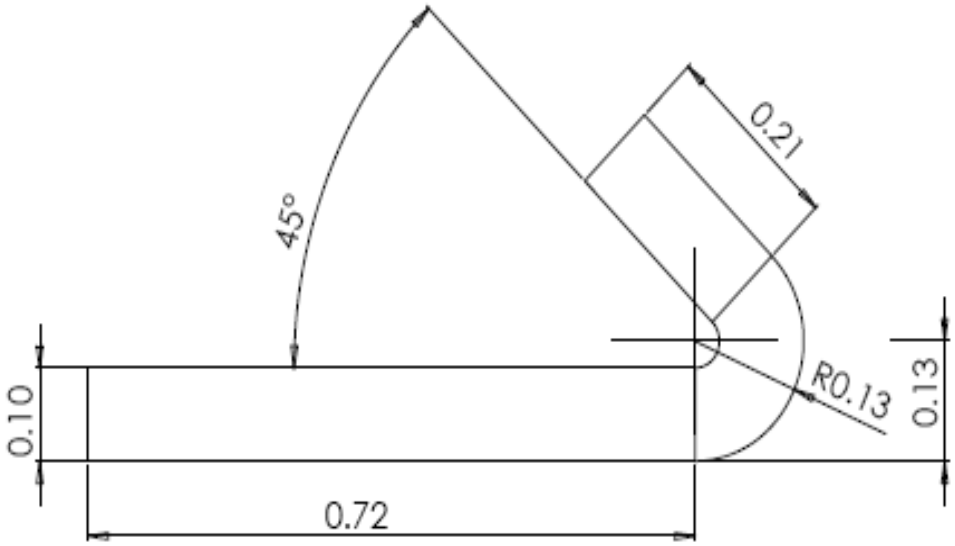

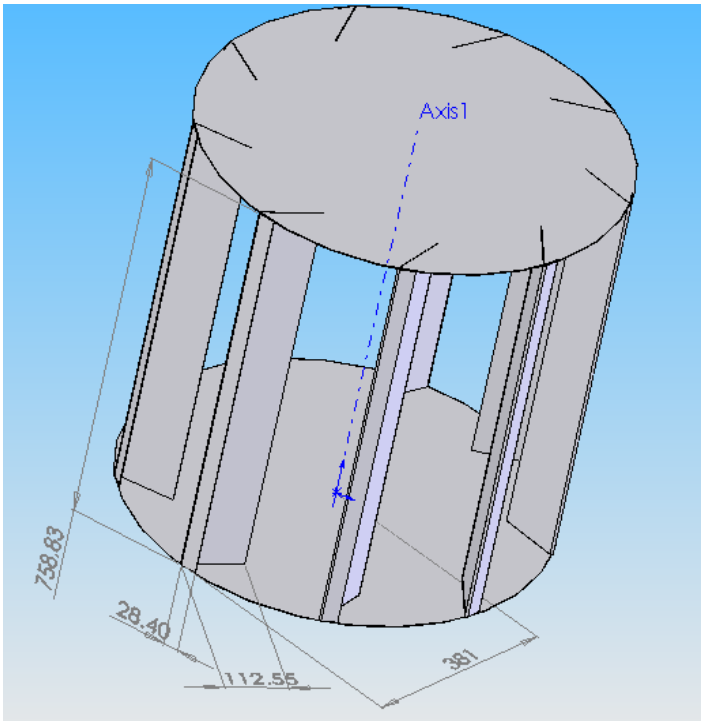

Isometric view of the stator-tab

Appendix F: Modified rotor – stator design dimensions.